Precambrian Research 427 (2025) 107879

Contents lists available at ScienceDirect

Precambrian Research

journal homepage: www.elsevier.com/locate/precamres

Lithostratigraphic, structural and geochronological framework of the Namibe region, SW Angola: Insights into the late Eburnean Orogeny in the Congo Shield

Javier Escuder-Viruete [a,*], Luis Quintana [a], Aratz Beranoaguirre [b], Pilar Montero [c], Janet Gabites [d], Pablo Valverde-Vaquero [a], Américo da Mata Lourenço Victorino [e]

[a] Instituto Geológico y Minero España, CSIC, C. La Calera 1, 28760 Tres Cantos, Madrid, Spain
[b] Institut für Geowissenschaften, Goethe-Universität Frankfurt, Altenhöferallee 1, 60438 Frankfurt am Main, Germany
[c] Laboratorio de Microsonda Iónica-IBERSIMS, Centro de Instrumentación Científica, Universidad de Granada, Granada, Spain
[d] Pacific Centre for Isotopic and Geochemical Research, University of British Columbia, 6339 Stores Road, Vancouver, BC V6T-1Z4, Canada
[e] Instituto Geológico de Angola, Kilamba, Luanda, Angola

ARTICLE INFO

Keywords:
Southwestern Congo Shield
Eburnean orogeny
Epupa Complex
Namibe Group
Structural analysis
Geochronology
Angola

ABSTRACT

The Namibe region in southwestern Angola represents the southernmost extent of the Southwestern Congo Shield; however, its tectonothermal evolution is still poorly understood. To better constrain the timing and deformation style of the outcropping rocks in this region, we integrated (i) 1:250,000-scale lithostratigraphic and structural geological mapping, (ii) SHRIMP U–Pb zircon dating of metamorphic rocks, and (iii) $^{40}Ar/^{39}Ar$ muscovite cooling ages. The study area comprises the Epupa Complex of ortho- and paragneisses, overlain by the Namibe Group, which is composed of supracrustal metasediments. The sharp lithological contrast, absence of orthogneisses, and the preservation of basal marbles suggest that the protoliths of the Namibe Group were unconformably deposited on the Epupa Complex. Both units experienced polyphase ductile deformation during the Eburnean event. Two penetrative deformation phases (D1 and D2) are overprinted by two later, less pervasive phases (D3 and D4). A subhorizontal D_2 shear zone links sinistral transpression in the upper crust with lateral flow in a partially molten lower crust. Peak metamorphic conditions led to widespread anatexis. SHRIMP U–Pb zircon ages from migmatitic leucosomes, granitic–tonalitic orthogneisses, and detrital to metamorphic zircons cluster tightly between 1.82 and 1.80 Ga, while $^{40}Ar/^{39}Ar$ muscovite ages indicate cooling at ~1.80 Ga. This implies that the thermal peak, melt segregation, granite emplacement, and cooling occurred within ≤10 Ma. The near-synchronicity of high-grade metamorphism and magmatism, together with the crustal-scale D_2 shear architecture, supports a model of hot, thickened crust undergoing vertical strain transfer during late Eburnean sinistral transpression. This study provides the first precise 1.82–1.80 Ga age bracket for the late Eburnean event in southwestern Angola, highlighting a well-preserved subhorizontal attachment zone that couples upper crustal shear with deep crustal flow.

1. Introduction

The Congo Shield in the Angola territory of constitutes one of the geologically least studied areas in southern Africa. The Archean-Paleoproterozoic basement and the overlying Paleoproterozoic supracrustal sequences remain poorly studied, preventing a comprehensive understanding of the geological and tectonic evolution of the Congo Shield. However, the recent Angolan government-sponsored geological mapping program (PLANAGEO; García Lobón et al., 2024), has enabled this situation to be reversed, improving the geological understanding of this region of the Southwestern Congo Shield. This is in particular for the Namibe region of southwestern Angola, where an extensive crustal block was subjected to tectono-metamorphic processes during the Eburnean orogeny.

As part of the outcome of the PLANAGEO, in this study we present the lithostratigraphy, structure and U-Pb/Ar-Ar geochronology of the metamorphic rocks in the Namibe region. These findings stem predominantly from the 1:250 000 scale geological mapping conducted in

* Corresponding author.
E-mail address: javier.escuder@csic.es (J. Escuder-Viruete).

https://doi.org/10.1016/j.precamres.2025.107879
Received 30 July 2024; Received in revised form 3 July 2025; Accepted 13 July 2025
Available online 15 July 2025

the Namibe and Muninho Quadrangles (Escuder-Viruete et al., 2021a; Gutiérrez-Medina, 2021). This mapping allows the following key objectives to be achieved for the first time: (1) establishing the lithostratigraphic relationships between the Epupa Complex and the Namibe Group in the Namibe region; (2) determining macrostructures and mesostructures resulting from the Eburnean deformation; and (3) constraining the precise Paleoproterozoic age of the regional deformation and metamorphism. Results from this study enhance the comprehension of the characteristics of the Eburnean orogeny in the Southwestern Congo Shield, giving light in particular to the meaning of the geometry and kinematics of the Eburnean deformation events, the timing of the thermal peak of the associated metamorphism and related processes of partial melting.

2. Geological setting

2.1. Cratons and shields of Central Africa

Following the terminology of Stankiewicz and de Wit (2013), "cratons" are defined as Archean crustal blocks that have been stabilized at > 2.5 Ga, whereas "shields" encompass post-Archean continental domains that were formed and/or amalgamated during specific periods of the Proterozoic-Phanerozoic times, and contain more or less deformed cratons. Basing on this terminology, the African continent comprises four major Precambrian Shields that include Archean craton cores subsequently deformed into Paleo- and Mesoproterozoic orogens and later amalgamated along Neoproterozoic orogenic belts (Lindeque et al., 2011).

The Angola territory includes several cratons of the Central African Shield. This shield is made of four cratons, namely (Fig. 1a): the Southwestern Congo Craton; the Central Congo Craton or Cuvette; the Northeastern Congo Craton or Mboumou-Uganda; and the Tanzanian Craton. Following de Wit and Linol (2015), the "Congo Shield" represents a vast lithospheric domain incorporating the first three cratons, which could not be directly linked beneath the Phanerozoic sedimentary basin of the Congo due to the discontinuity of the rock exposures. These cratons were amalgamated during the Proterozoic and are located within or surrounded by Eburnean (ca. 2.3–1.8 Ga), Kibaran (ca. 1.4–1.0 Ga), and Pan-African (ca. 0.8–0.5 Ga) orogenic belts.

During the middle Paleoproterozoic, the northern and eastern boundaries of the Congo Shield were convergent continental margins where subduction and obduction of oceanic lithosphere occurred between 2.3 and 2.0 Ga, as well as the accretion of Archean continental fragments between 2.05 and 1.88 Ga (Boniface and Schenk, 2012; Boniface et al., 2012; Nkoumbou et al., 2013; Lawley et al., 2013, 2014; de Wit and Linol, 2015). The southern edge of the Congo Shield is delineated by the Central Angola Mobile Belt (Fig. 1b; de Wit and Linol, 2015), partially corresponding to the "Central Angola Shield Zone" (Carvalho et al., 2000). This region represents a broad orogenic zone characterized by Eburnean deformation and metamorphism, widespread granitic magmatism and the occurrence of fragments of reworked Archean crust (Doucoure et al., 1999; Carvalho et al., 2000; Jelsma et al., 2011, 2018). This orogenic belt marks the collisional zone between two crustal blocks that amalgamated at 2.0 Ga to form the Southwestern Congo Shield (Wit and Linol, 2015).

Between the Congo Shield and the Tanzanian Craton there lies a vast region of Proterozoic basement, encompassing Eburnean (referred to as Ubendian here), Kibaran, and Pan-African orogenic belts (Holmes, 1951). The Eburnean collisional zone includes the Ruwenzori Fold Belt (Tanner, 1974) and the Buganda-Toro System (Nagudi et al., 2003), that sutured the Northeastern Congo Craton (Mboumou-Uganda) to the Archean Tanzanian Craton (Fig. 1). In the southwestern margin of the Tanzanian Craton, high-P metamorphic belts were accreted during the 1868–1866 Ma subduction of oceanic crust (Boniface et al., 2012; Kabete et al., 2012a and b; Lawley et al., 2013, 2014). This metamorphic belt was later reworked during the Kibaran and Pan-African orogenic

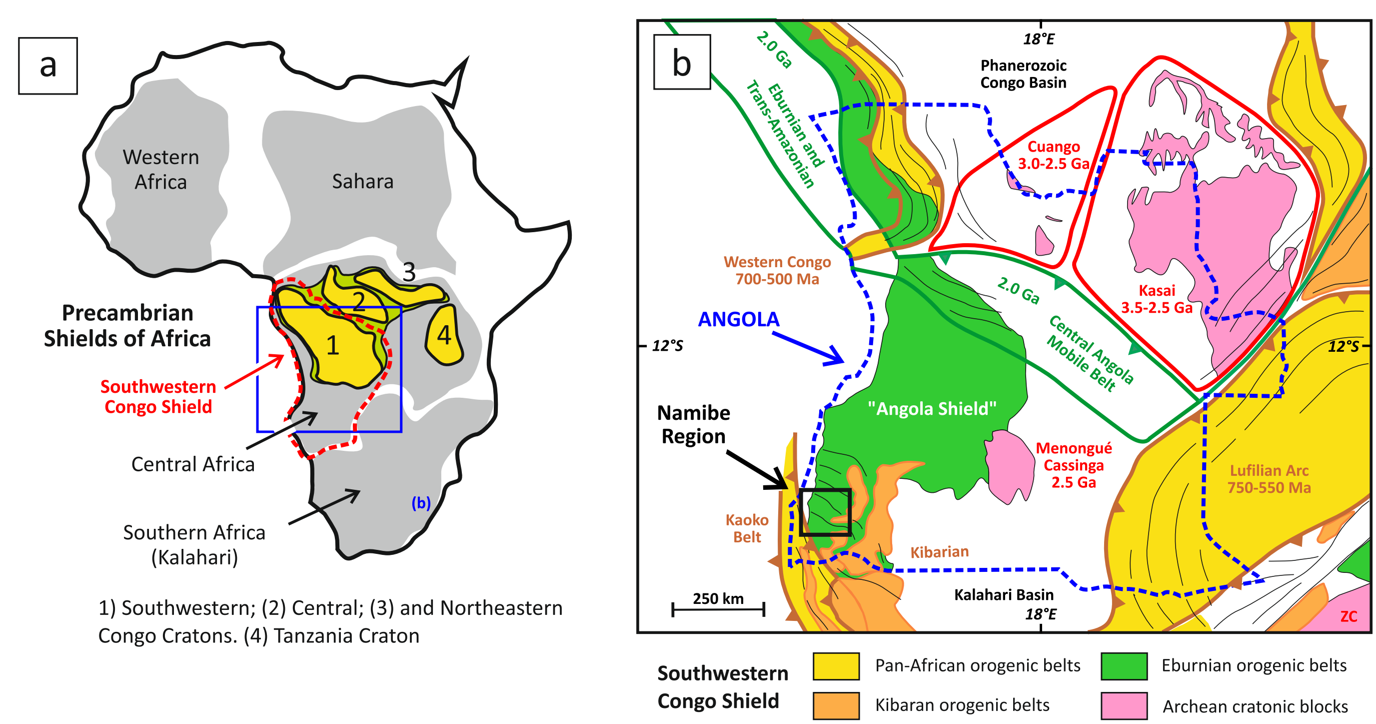

Fig. 1. (a) Simplified map of the Precambrian Shields of Africa (Lindeque et al., 2011). The Central African Shield comprises the following cratons (yellow): (1) Southwestern Congo Craton; (2) Central Congo Craton or Cuvette; (3) Northeastern Congo or Mboumou-Uganda Craton; and (4) Tanzania Craton. The dashed red line marks the boundary of the Southwestern Congo Shield, which includes the Archean Ntem, Cuango and Kasai cratons. (b) Diagram of the Precambrian basement surrounding the Phanerozoic Congo Basin (modified from de Wit and Linol, 2015), showing Archean cratonic blocks (purple), Eburnian (green) and Kibaran/Pan-African (orange and yellow) terranes, as well as the orogenic fronts of the Pan-African fold and thrust belts (brown). ZC; Zambia Craton. Thin black lines show direction of regional foliation. The purple line defines the administrative limits of Angola.

events.

The subsequent accretion of crustal blocks along the orogenic belts surrounding the Congo Shield was responsible for the evolution of the "Central African Shield", which stabilized during the late Neoproterozoic to early Cambrian times (Fig. 1a, b). This Shield encompasses several Pan-African structures, including: the Western Congo Belt of Gabon, Democratic Republic of Congo and northwestern Angola; the Oubanguides of northern Gabon and Cameroon; the Mozambican Belt of South Sudan, eastern Tanzania, Kenya and Mozambique; the Lufilian Belt (or Arc) of Zambia and its extension into southwestern Angola and northwestern Botswana and Namibia as the Damara Belt, further continuing northward through the Kaoko Belt and into the Western Congo and the Araçuaí Brazilian Belts (Master et al., 2005; Milesi et al., 2006; de Wit et al., 2008; Waele et al., 2015; Thiéblemont et al., 2016; Degler et al., 2017).

2.2. The Eburnean Orogeny in the Southwestern Congo Shield

The Southwestern Congo Shield comprises the Ntem, Cuango and Kasai Archean cratons, as well as a broad crustal domain situated further southwest in Angola, predominantly consisting of Eburnean and Kibaran crust (Thiéblemont et al., 2018; Fig. 1b). Within this domain, a 200 km-wide and NW-SE trending Central Angola Mobile Belt is characterized by intense Eburnean ductile deformation, amphibolite to granulite facies regional metamorphism and extensive granitic plutonism, as well as reworked Archean greenstones and granitoids (Carvalho et al., 2000; de Wit and Linol, 2015; Jelsma et al., 2011, 2018). According to Jelsma et al. (2011, 2018) and de Wit and Linol (2015), this belt represents the root of an Eburnean collisional orogen, formed as a result of the southward underthrusting of the Kasai Craton beneath the "Angola Shield", leading to the formation of the Southwestern Congo Shield.

North of the Central Angola Mobile Belt, the Cuango and Kasai Cratons were affected by Eburnean tectonometamorphism. In this sector, the Mubindji event (2.2–2.0 Ga) deformed the Paleoproterozoic metasedimentary rocks of the Luiza Group and the pillow-lava metabasalts of the Lulua Group. These supracrustal rocks were deposited unconformably onto Archean charnokites (Cahen et al., 1984; Carvalho et al., 2000). South of the Central Angola Mobile Belt, the Archean-Paleoproterozoic metamorphic rocks extends several hundred kilometers to the tectonic boundary with the Kaoko Belt in Namibia, featuring remnants of Archean gneisses (2.62–2.58 Ga; Cahen et al., 1984; Carvalho et al., 2000) interspersed between Eburnean granitoids (Miller, 2008a and b).

In the southwestern region of Angola, the Archean-Paleoproterozoic basement is unconformably overlain by the Chela Group of late Paleoproterozoic metasedimentary rocks (McCourt et al., 2004, 2013; Pereira et al., 2013), and intruded by the Mesoproterozoic Cunene Mafic-Anorthositic Complex (1.44–1.37 Ga; Drüpel et al., 2007; Maier et al., 2013; Lehmann et al., 2020). According to De Wit and Linol (2015), the Central Angola Mobile Belt was displaced by a NE-trending, left-lateral strike-slip shearing Eburnean-Kibaran event, extending further northwest in the Eburnean Belts bordering the Tanzanian Craton.

2.3. Geology of the Namibe region

The plutono-metamorphic basement exposed in the southwestern region of Angola has traditionally been known as the "Angolan Shield" (Araújo et al., 1988; Araújo and Guimarães, 1992), including rocks of Archean, Paleo-, and Neoproterozoic age. This unit includes a portion of the Southwestern Congo Shield (Jelsma et al., 2011, 2018), bounded to the north by the Archean to Neoproterozoic rocks of the Kwanza Horst, to the east by the Mesozoic to Cenozoic continental deposits of the Congo and Kalahari Basins, and to the west by the Lower Cretaceous to Quaternary coastal and marine deposits associated to the opening of the South Atlantic Ocean. Located in the "Angolan Shield", the Namibe region includes lithologically the "Complexo Gnaissico-Migmatitico e Granitico" (Carvalho, 1983, 1984), which groups a collection of variably migmatized gneisses intruded by anatectic granites and granitic pegmatites. This assemblage is overlain by the greenschist facies "Complexo Xisto-Quartzitico-Anphibolitico" (Carvalho, 1983; 1984; Pereira et al., 2011, 2013). Traditionally, both units are considered together as an Archean "base complex", strongly reworked during the Eburnean orogeny (Carvalho, 1984). The Eburnean reworking is confirmed by the U-Pb zircon ages of migmatization of gneisses at 1776 ± 13 Ma and 1783 ± 32 Ma, as well as crystallization of anatectic granites at 1744 ± 9 Ma in the Chibia region (Pereira et al., 2013).

In the Cunene River region along the border of Angola and Namibia, the Epupa Complex (Tegtmeyer and Kröner, 1985) comprises the granulite facies metasedimentary and metavolcanic rocks of the Epembe unit, and the amphibolite facies orthogneisses and paragneisses of the Orue unit (Brandt et al., 2003, 2007, 2008; Seth et al., 1998, 2003, 2005). The U-Pb zircon ages for the orthogneissic protoliths of the Epupa Complex range from 1795 ± 30 Ma (Tegtmeyer and Kröner, 1985), 1775 ± 1 Ma (Kröner et al., 2010), between 1861 ± 3 Ma and 1758 ± 3 Ma (Kröner et al., 2010, 2015), and 1773 ± 20 Ma (Ruacana granite augen-gneisses, Escuder-Viruete et al., 2021c). Ages obtained in Namibia for the migmatitic foliation and related synkinematic anatectic granites are 1778 ± 4 Ma, 1762 ± 4 Ma and 1754 ± 4 Ma in the Orue unit (U-Pb in zircon; Kröner et al., 2010, 2015), and range between 1740 and 1720 Ma in the Eyao unit (SHRIMP U-Pb in zircon; Brandt et al., 2021). They establish deformation and upper amphibolite facies metamorphism of the Epupa Complex protoliths during a late Eburnean orogenic event. Based on their similar lithology and ages, the gneisses of the "Complexo Gnaissico-Migmatitico e Granitico" can be correlated with those of the Epupa Complex, recording a granitic magmatism subsequently affected by the late Eburnean tectonometamorphism. Subsequently, the Epupa Complex underwent a local granulite facies metamorphic overprint during the Mesoproterozoic emplacement of the Cunene Gabro-Anorthositic Complex (1490–1447 Ma; Pb-Pb in garnet; Seth et al., 2003, 2005), and amphibolite facies metamorphism associated to the intrusion of Mesoproterozoic granitoids (1390–1320 Ma; U-Pb in zircon; Brandt et al., 2003; Seth et al., 2003, 2005; Brand and Klemd, 2008; Kröner and Rojas-Agramonte, 2017; Brandt et al., 2021; Milani et al., 2022).

3. Lithostratigraphy

The Namibe region is characterized by two distinct Precambrian lithological assemblages: (1) an association of Paleoproterozoic metamorphic rocks, including the Epupa Complex and the supracrustal metasediments of the Namibe Group; and (2) a group of Paleoproterozoic granitoids classified as syn-, late- and post-kinematic on the basis of their structural relationships with the main Eburnean deformation episode (Escuder-Viruete et al. (2021a, 2024a, b). Both lithological assemblages are intruded by Mesoproterozoic mafic dyke systems. Toward the west, Paleoproterozoic rocks are unconformably overlain by Cretaceous to Cenozoic sedimentary and volcanic rocks of the Namibe Basin, as well as surface deposits of Quaternary age. The spatial distribution of these lithological assemblages is illustrated in the geological map of the Fig. 2.

3.1. Epupa Complex

The Epupa Complex in the Namibe region comprises a variety of lithologies, including variably migmatized granitic orthogneisses, paragneisses, and less-abundant tonalitic and dioritic orthogneisses. The granitic orthogneisses exhibit a compositional banding defining the main foliation (S2), characterized by alternating quartz-feldspathic and relatively thin biotitic-sillimanitic layers. An earlier foliation (S1) is identified by the alignment of biotite within S2 microlithons and elongated inclusions in porphyroblasts. At outcrop scale, different facies of granitic orthogneisses are recognized, including augen-gneisses

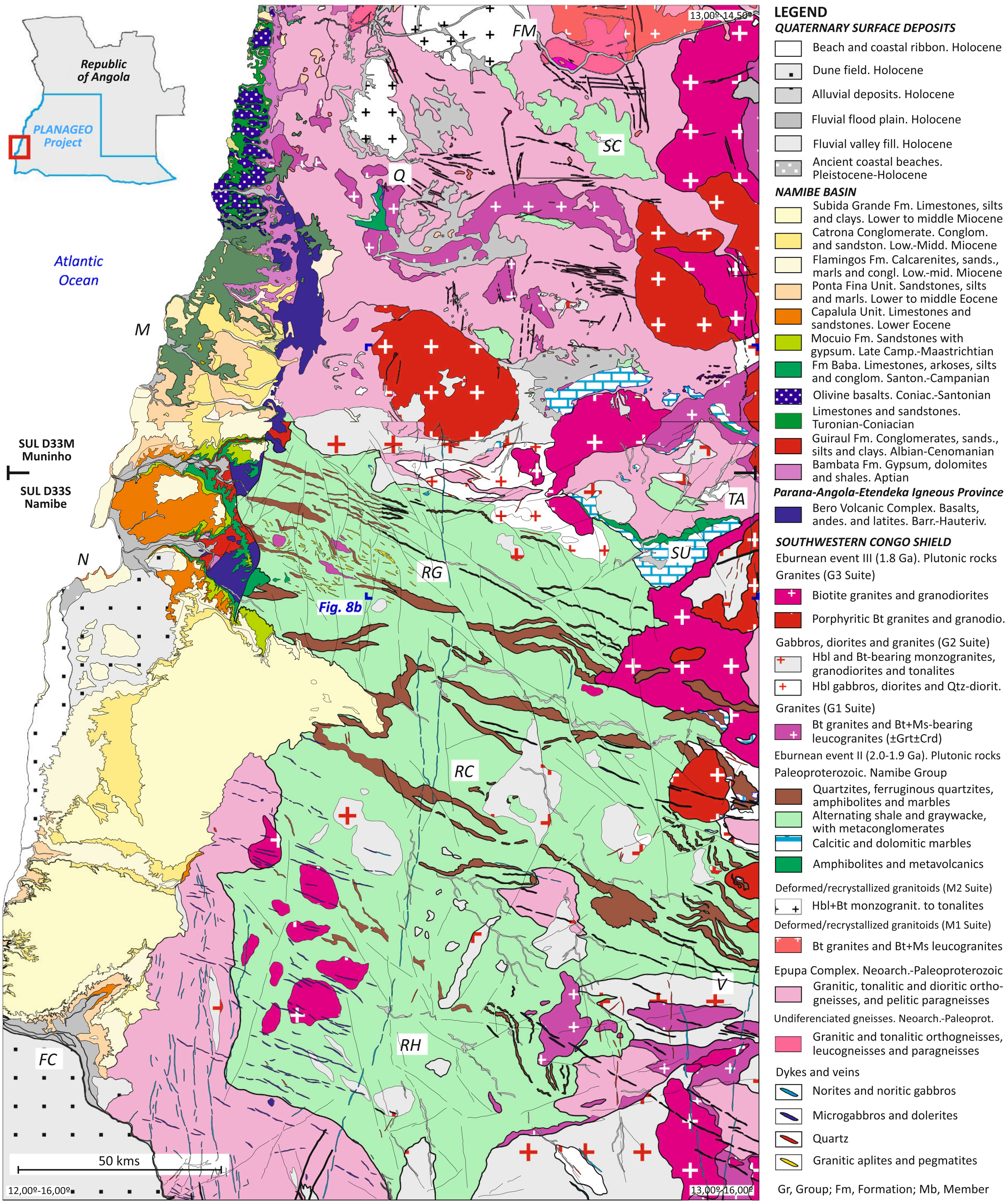

Fig. 2. Schematic geological map of the Namibe (Sul D-33/S) and the southern half of the Muninho (Sul D-33/M) Sheets at E.1:250 000 (modified from Escuder-Viruete et al., 2021a; Gutiérrez-Medina, M., 2021). Thin black lines indicate faults. CF; Façenda Curoca, FM; Façenda Maungo, M; Mucuio, N.; Namibe, V; Virei, Q; Quitungua, R. C.; Cubai river valley; RG; Giraul river valley; RH; Hiquia river valley, SC; Serra da Chicallungo, SU; Serra Uimpa; TA; Tchicolangite antiform.

(Fig. 3a), banded orthogneisses (Fig. 3b, c) and felsic orthogneisses with low biotite content. The granitic orthogneisses are in most places structured in centimeter-thick, leucosome-melanosome pairs parallel to the main foliation (S2), giving rise to a stromatic structure. Mineralogically, they comprise quartz, plagioclase and K-feldspar, with varying proportions of biotite, sillimanite, cordierite and garnet, as well as retrograde muscovite. The tonalitic orthogneisses display a penetrative compositional layering (S2) of alternating flattened quartz-feldspathic lenses and biotite and in places hornblende-rich levels. The quartz-feldespatic lenses are frequently leucosomes with biotite and/or amphibole-rich selvages. The dioritic orthogneisses exhibit banded structures (S2) defined by alternating quartz-plagioclase and biotite-amphibole-rich layers. At the outcrop scale, a transition from non-migmatitic orthogneisses to metatexitic orthogneisses characterized by development of leucosomes parallel to the main S2 foliation is common. Diatexitic and nebulitic gneisses contain a greater content of melt, which forms pockets of leucosome cutting the S2 foliation. The diatexites exhibit a gradation to heterogeneous granitoids rich in biotitic schlieren structures. When these melts acquire a certain degree of mobility, they form more homogeneous leucogranites of medium to coarse grain size

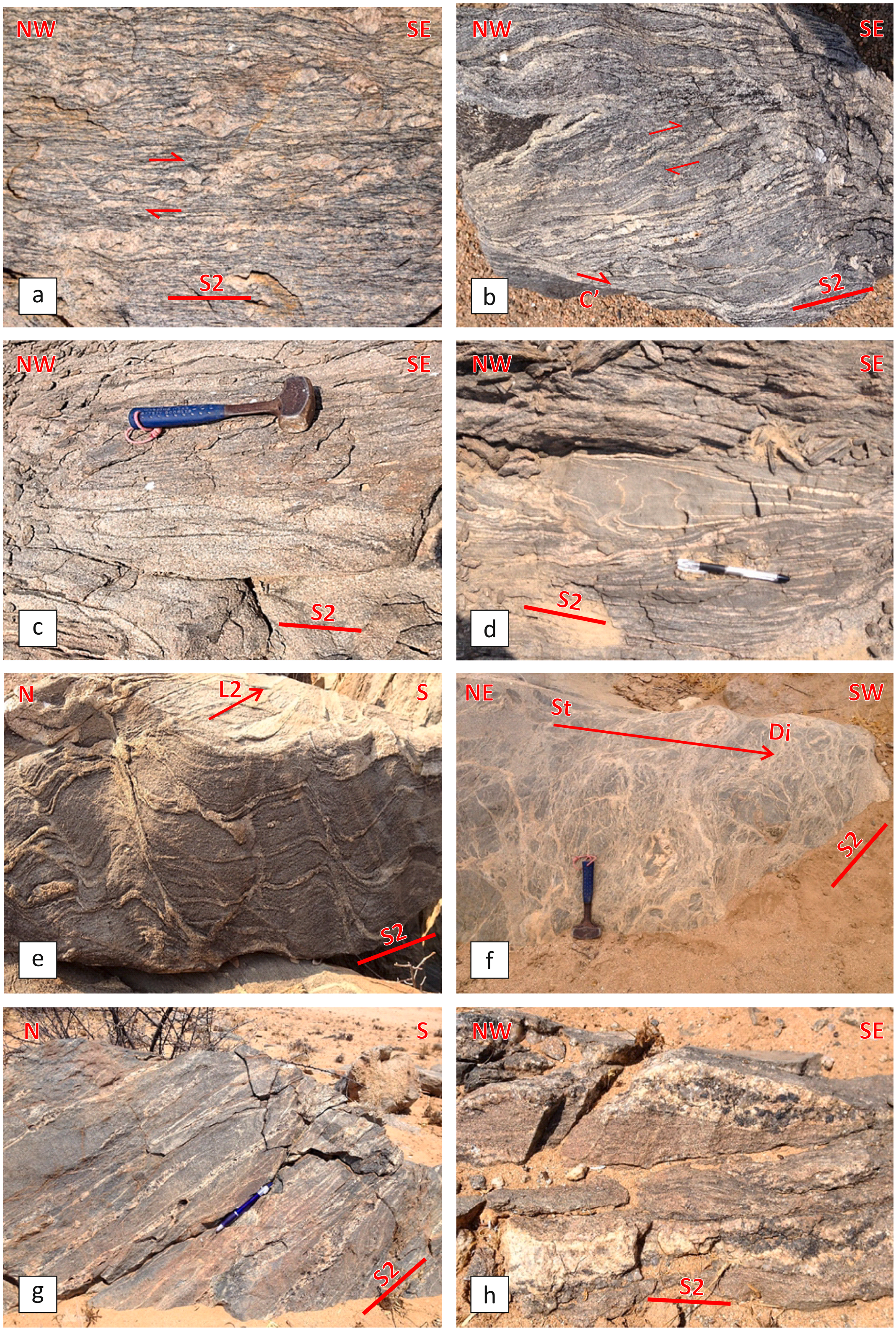

Fig. 3. (a) Granitic augen-gneisses of the Epupa Complex. Note the porphyroclastic character of the feldspar megacrystals in a blastomylonitic matrix (S2). Curoca sector. (b) Biotitic banded orthogneisses, with leucosomes (S2) sheared and deformed by C' planes. Road from Curoca to Iona. (c) Biotitic banded orthogneisses with concordant intrusions (S2) of anatectic leucogranites. Road from Curoca to Iona. (d) Semi-pelitic paragneisses with stromatic structure (S2) deformed by D3 folds. Curoca sector. (e) Tonalitic orthogneisses with several generations of syn- and post-S2 leucosomes, some of them elongated defining a mineral lineation (L2). Tchicolangite antiform. (f) Transition from stromatic (St; left) to diatexitic (Di; right) structures in semi-pelitic paragneisses, as the volume of granitic melt increases. SW sector of the Kanahuia benchmark, Virey. (g) Stromatic paragneisses with development of leucosomes parallel to the S2 foliation, which are heterogeneously boudinaged and isoclinally folded. Capolopopo antiform. (h) Stromatic paragneisses with development of elongated leucosome-melanosome pairs parallel to the S2 foliation. Mongobatú sector, Capolopopo. In the photographs, the field width is 60 cm and the arrows indicate the D2 shear sense viewed in the XZ plane of finite strain (i.e., perpendicular to the shear plane and parallel to stretching lineation).

(e.g., G1 suite of syn- to late-D2 granitoids of Escuder-Viruete et al., 2021a, 2024a, b).

The paraderived rocks comprise of stromatic biotite-rich paragneisses (metapelites), biotite-sillimanite schists, graphitic black schists, feldspathic metasandstones and quartzites. The contact between the paraderived rocks and orthogneisses is net, often characterized by flattened biotite and sillimanite-rich enclaves in the orthogneisses near the contact. The latter indicates that the biotite and sillimanite-rich paragneisses were intruded by the protoliths of the orthogneisses. Unlike the Namibe Group, there are no observed intercalations of marble or amphibolite. Stromatic paragneisses exhibit a leucosome-melanosome pair structure (Fig. 3d to h), leading a gneissic banding (S2). Mineralogically, this banding is defined by alternating quartz-feldspar and biotite-sillimanite-rich layers. The associated mineral lineation (L2) is defined by the elongation of acicular sillimanite nodules, cordierite and garnet porphyroblasts, and polycrystalline quartz aggregates. Biotite-sillimanite schists display a planar-linear fabric (S2-L2), defined by the parallel arrangement of biotite sheets and elongate sillimanite aggregates. The paragneisses contain quartz, plagioclase, biotite, and sillimanite, with varying proportions of K-feldspar, cordierite and garnet, and retrograde muscovite. In the feldspathic metasandstones and quartzites, the S2 foliation is defined by elongate quartz-feldspathic aggregates and the preferential orientation of the biotite and ilmenite crystals.

3.2. Namibe Group

The Namibe Group comprises a basal section of amphibolite and calcitic/dolomitic marble, overlain by slates, quartz-rich schists, quartz-felspathic schists and metagraywackes (Figs. 2, 4a to h). The metaconglomerates, quartzites, ferruginous quartzites and schists of the Sierra de Chicallungo are included in the Namibe Group due to their lithological similarity (Gutiérrez-Medina, 2021). On the basis of the lithological characteristics and preserved sedimentary structures, three geographical sectors can be distinguished in the Namibe Group, namely northeastern, central and southwestern.

In the central sector (Serra Uimpa; Fig. 2), the amphibolite and marble basal section ranges between 100 and 150 m in thickness (Fig. 2). Amphibolites are medium to fine grained, olive-green rocks with a massive or banded structure and a penetrative planar-linear fabric (S1-L1 or S2-L2; Fig. 4g), characterized by alternating amphibole and plagioclase-rich layers. A mineral lineation is defined by the elongation of amphibole prisms. The presence of folded and boudinaged amphibolite layers in the calcitic marbles in the Chaco-Chaco sector (Fig. 4h) suggests that the protoliths of these rocks are in part mafic dikes or sills, which intruded at the base of the Namibe Group metasedimentary sequence., Gutiérrez-Medina (2021) describes the presence of intercalations of mafic and felsic metavolcanic rocks in the basal section of the Munhino sector. Metacarbonate rocks on the flanks of the Tchicolangite antiform (Fig. 2) form a 250–300 m-thick section of alternating calcitic and dolomitic marbles, with intercalations of decametric-thick levels of calc-schists and calc-silicate gneisses. Marbles at the outcrop scale are white, yellow or greenish-gray colored rocks, displaying a poorly marked compositional banding (S1 or S2) of elongated calcite or dolomite grains.

The dominant lithological association of the Namibe Group consists of alternating shales and metagraywackes with intercalations of lenticular-shaped metaconglomerate beds. This siliciclastic sequence is very monotonous and has an estimated thickness of several thousand meters, orthogonal to the main foliation. In the northeastern sector (Serra da Chicallungo), the sequence comprises basal polymictic metaconglomerates (Fig. 4c) overlain by alternating meter-thick beds of quartzites, ferruginous quartzites and metagraywackes. Metaconglomerate beds have erosive bases and lenticular geometries, containing granite and quartzite pebbles (Fig. 4d). Quartzite and metagraywacke exhibit graded internal sedimentary structures with sporadic development of Bouma sequences. This lithologic association corresponds to the typical coarse-grained clastic sedimentation in the channeled part of a turbiditic depositional system. (e.g., Bouma, 2004).

In the central sector (Giraul and Cubal rivers valleys; Fig. 2), the sequence includes basal amphibolite and metacarbonate rocks, overlain by an alternance of slate, phyllite, quartz-schist, metagraywacke and quartzite. Metasandstone beds range between 10 cm to 1 m in thickness with frequent cyclicity in their variation, forming sections of decametric thickness. The metaconglomerates define lenticular beds, generally less than 50 cm in thickness, composed of centimeter-sized quartz clasts and slightly altered feldspars. The typical arkose matrix of the metaconglomerates (Fig. 4e) is indicative of a rapid transport by turbidity currents. The sedimentary structures preserved in the metasandstone beds are characteristic of turbiditic deposits. They include irregular erosive bases, decreasing grain size upwards, parallel lamination and current ripples on top. Locally, there is amalgamation of layers by synsedimentary erosive processes. The lithological association is typical of medium- to coarse-grained siliciclastic sedimentation in proximal lobes of the unchanneled part of a turbiditic depositional system (e.g., Bouma, 2004).

In the southwestern sector (Hiquia river valley; Fig. 2), the sequence comprises phyllites and slates, with sporadic intercalations of quartz-poor metagraywacke, quartz-rich metagreywacke and quartzite (Fig. 4f). Metasandstone layers vary in thickness between 1 to 15 cm and are often grouped into 10 to 100 m-thick sections showing internal cyclicity in bed thickness. Slate and graphite-rich metapelite are locally intercalated to form homogeneous sections of decametric thickness. Sedimentary structures include decreasing grain size upwards, current ripples and parallel lamination. These structures, together with the general fine granulometry and lower thickness of the metasandstone beds, point to sedimentation in the distal part of the turbiditic depositional lobes (Bouma, 2004).

The succession of slates and metagraywackes intercalates sections of quartzite, ferruginous quartzite and paraamphibolite. These quarzitic-rich sections vary in thickness from 10 to 150 m and can laterally grade to metagraywacke beds. Ferruginous quartzite and quartzite form 10 cm to 2 m-thick layers characterized by a lenticular geometry. Beds exhibit an internal upwards decrease in grain size and parallel to cross laminations on top. These features are indicative of excavation and progressive filling of channels in the proximal part of the turbiditic system. Amphibolites and impure marbles form 10 to 80 m-thick competent sections intercalated in the slates, which can pinch-out laterally. They occur isolated or associated with layers of quartzite. These intercalations have been related to episodic deep marine carbonate sedimentation (Escuder-Viruete et al., 2021a).

4. Structure

4.1. Regional macrostructure

Eburnean structures identified in metamorphic rocks of the Namibe region are grouped into two main ductile deformational events, namely D1 and D2, and two subsequent, less pervasive events, namely D3 and D4. Deformation D1 was related with a sinistral transpressive deformation (see below), which formed a subvertical S1 planar fabric and an accompanying L1 lineation. Depending on the lithology and strain and metamorphism intensity, S1 is manifested as slaty cleavage or schistosity in metapelites, a coarse or discontinuous schistosity in competent metasandstones, or a foliation in recrystallized metacarbonate rocks.

Fabrics and structures developed during D1 were variably overprinted and transposed at all scales by structures linked to the D2 event. These structures developed at the lower structural levels of the Namibe Group and across the exposed Epupa Complex (Fig. 5 and geological cross-sections of Fig. 6). The D2 deformation gave rise to a kilometer-thick band of metamorphic rocks characterized by a pervasive planar-linear fabric (S2-L2), with an original subhorizontal disposition. S2

NW

Fig. 4. (a) Panoramic view of the southern flank of the Tchicolangite antiform in which the lower gneisses of the Epupa Complex (CE) are overlain by the basal amphibolites (Am) and marbles (Ma) of the Namibe Group. Amphibolites and marbles form a homoclinal sequence inclined to the south. Cuanhangue Peak, Caraculo-Virey road. (b) Centimeter-scale alternance of schist and metagraywacke beds (S0) typical of the Namibe Group. Note the less penetrative development of the primary S1 foliation in the metasandstone beds. Hiquia Sector SW of Virey. (c) Panoramic view of the basal conglomerates of the Namibe Group with development of the S1 foliation. Quitungua sector. (d) Rounded clasts of the polymictic basal conglomerates of the Namibe Group surrounded by the S1 foliation. (e) Metagraywacke bed with a basal microconglomerate rich in quartz and feldspar clasts. Note the subvertical dip of the S1 planes. Namibe Group along the Virey-Cainde road. (f) Panoramic view of the alternance of metagraywackes and phyllites of the Namibe Group. Note the high-dip angle of S1 foliation. Giraul river valley in Chinda. (g) Amphibolite with a compositional banding (S2) deformed by NE-vergent D3 folds. Fold-axes plunging a low-angle to the SE. Caraculo-Virey road. (h) White calcitic marbles (Ma) intruded by an amphibolitized mafic dike (Am), deformed by D2 folds. Southern slope of Cuanhangué, on the Caraculo-Virey road. Field width = 4 m.

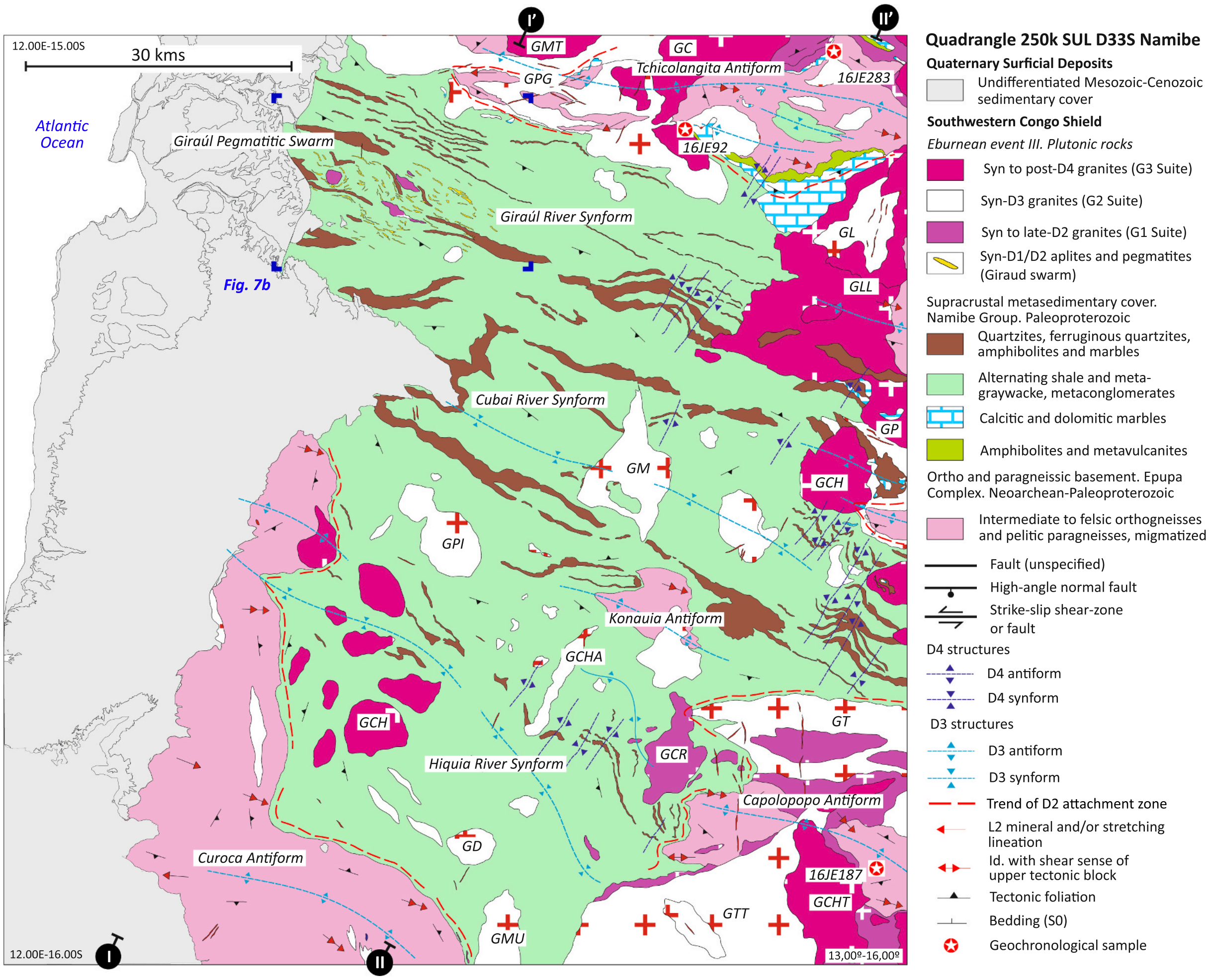

Fig. 5. Main Eburnean macrostructures in the Namibe (Sul D-33/S) Sheet at 1:250 000 scale (modified from Escuder-Viruete et al., 2021a). GMT; Monte Tubirute granites, GC; Caraculo granites, GPG; Piedra Grande granites, GLL; Linda Linda granites, GL; Laué granites, GP; Picona granites, GCH; Chintangala granites, GM; Macala granites; GPI; Pico granites, GCHA; Chamacuala granites, GT; Tulandjo granites, GCH; Caraué granites, GCHT; Chitundulu granites, GTT; Teteombe granites, GMU; Mupavia granites; GD; Dalundo granites, GCH; Camahaha granites.

fabric is a schistosity defined by quartz-mica compositional banding in the lower structural levels of the Namibe Group, whilst appears as a gneissic to migmatitic foliation in the Epupa Complex. Structurally, the formation of the S2 fabric is associated with a major low-angle ductile shear zone. This shear zone gave rise to the vertical partitioning of the D2 deformation in the crust with the separation of the overlying metasedimentary cover from the underlying gneissic basement.

The late ductile D3 and ductile–brittle D4 deformations played a crucial role in shaping the final regional macrostructure as the rocks reached shallower crustal levels. This macrostructure comprises alternating antiforms and synforms developed during the D3 deformation, folded subsequently into transverse bands by the D4 deformation. In the Namibe region, the main D3 antiformal macrostructures are Tchicolangite, Konauia, Capolopopo and Curoca antiforms, which exhibit a WNW-ESE to W-E trend (Fig. 5). These structures have a 2–10 km short-axis dome-shaped geometry, defined by the folding of the S1/S2 foliation and the contact between the overlying Namibe Group and the underlying Epupa Complex in the core (Fig. 6a). Within the metasedimentary rocks of the Namibe Group, several D3 synformal structures composed of several lower-order antiform-synform pairs separate the regional antiforms. The Chicallungo, Giraúl River, Cubai River and Hiquia River are the main large-scale synforms (Fig. 5). The D3 deformation also generated WNW to W-striking sinistral subvertical shear zones, primarily developed in hinge zones and limbs of the antiformal domes. The axial planes of the D3 macrostructures often exhibit a sigmoidal cartographic trace due to the NNE-trending folding produced by the subsequent D4 event.

During the Eburnean deformation, granitic magmas predominantly intruded along the regional amphibolite-facies D3 antiformal areas (Escuder-Viruete et al., 2021a). Diverse granitoid timing of emplacement relative to the deformational events and magma composition led to distinctive plutonic suites (Fig. 5). They include syn- to late-D2 foliated granites and leucogranites (G1 peraluminous suite), late-D2 to essentially syn-D3 gabbros, diorites and granites (G2 metaluminous suite), and syn- to post-D4 granites (G3 metaluminous suite). U-Pb CA ID-TIMS zircon geochronology of these granitoids reveals a short time spam of ca. 10 Ma for plutons emplacement with distinctive pulses at 1808 Ma (G1-G2 suites) and 1803–1801 Ma (G2-G3 suites) (Escuder-Viruete et al., 2024a, b).

4.2. Mesostructures and mineral assemblages

4.2.1. Bedding S0

Bedding (S0) is exclusively preserved in the metasedimentary rocks of the Namibe Group less affected by Eburnean deformation and metamorphism. While the orientation of the S0 planes displays significant dispersion, there is a prevalent occurrence of NE to E-striking planes with > 60° dip angles towards the S and SE and WNW-striking planes with mid-dip angles ranging between 30° and 60° towards the SW, as well as subhorizontal planes (Fig. 6b). The S0 average pole is oriented

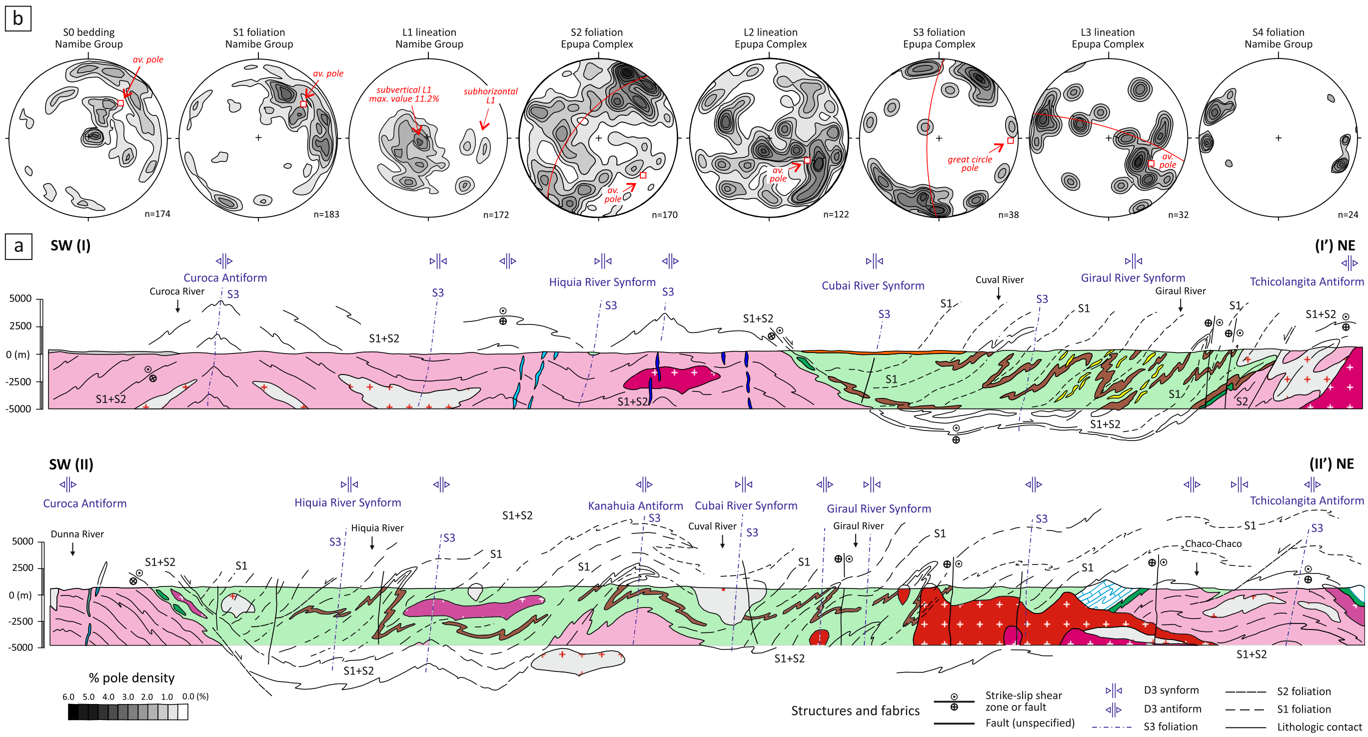

Fig. 6. (a) Schematic geological cross-sections of the Namibe region (modified from Escuder-Viruete et al., 2021a). Legend and location are shown in Fig. 5. (b) Stereographic projection of poles of planar and linear structural elements of different deformational events. See a detailed explanation in the text.

N036°E, with a plunge of 44° to the NE. The dispersion of these planes suggests that the S0 bedding was folded along WNW to NW-trending fold-axes associated with D1 and subsequent deformations.

4.2.2. D1 deformation

Syn-metamorphic D1 deformation was responsible for the folding of the metasedimentary rocks of the Namibe Group. Cartographic traces of the D1 folds and stereographic projection of the D1 structural fabrics developed in the eastern part of the Giraul River Valley are illustrated in the Figs. 6b and 7a, b. D1 folding gave rise to a system of kilometer-scale asymmetric anticlines and synclines with a WNW to NW trend and general NE vergence, which is particularly evident in the competent metasandstone layers of the Namibe Group (Fig. 6a). The axial-plane S1 foliation exhibits a relatively consistent WNW to NW trend and a medium to high-dip angle towards the SW (Fig. 6b). The S1 average pole orientation is N057°E plunging 25° to the NE. The intersection of the S0 and S1 planes defines an NNE to NE-trending lineation L1, often characterized by a steeply plunging to the SW (Figs. 6b, 7c, d). The axes of the D1 mesoscopic folds have a similar orientation to that of L1.

Centimetric-scale quartz and calcite veins developed during D1 folding, often defining *en-chelon* patterns. These veins generally exhibit a WNW to NNW orientation and a steeply dipping to the SW. Veins underwent shearing and folding along subvertical axes, rotating towards parallelism with the S1 foliation during progressive D1 deformation (Figs. 7d, 8a, b). Folding asymmetry and sense of rotation of the vein arrays establish a subvertical left-lateral shear. These structures account for the sinistral transpressive character of D1. A NW-SE to WNW-ESE trending subhorizontal L1 lineation has also been observed in high-strain shear bands (Fig. 6b). D1 deformation developed in the metasedimentary rocks of the Namibe Group under low-P greenschist to amphibolite facies regional metamorphic conditions. In phyllites and schists, S1 is defined by a fine-grained granolepidoblastic aggregate of quartz, albite, muscovite, biotite and opaque minerals, with variable modal contents of chlorite, cordierite, andalusite, staurolite and garnet (Fig. 8e, f). These mineral associations in metapelites allow local mapping of the syn-D1 prograde mineral isograds of biotite, garnet and staurolite (Escuder-Viruete et al., 2021a). The spatial arrangement of these isograds defines an increase in the field metamorphic gradient towards the lower structural levels of the D1 macrostructures.

4.2.3. D2 deformation

In the lowermost structural levels of the Namibe Group and the Epupa Complex the main foliation S2 is defined by a gneissic to migmatitic banding structure. The early S1 foliation is preserved in S2 microlithons and D2 fold hinge zones. The S2 gneissic foliation presents a main WNW to NW trend with a medium to high-dip angle to the NE and SW, both in the Namibe Group and in the Epupa Complex, despite a large dispersion in its orientation (Figs. 6b, 7a, 9a). S2 poles align along a N218°E striking plane dipping 66° to the NW, whose pole has a low-angle of plunge to the SE, similar to the D3 fold-axes. These structural relationships indicate S2 foliation to have been folded to form antiforms and synforms during D3, as can also be deduced from the detailed geological map of the Tchicolangita sector in the Fig. 9b. The associated stretching and/or mineral lineation L2 exhibit a predominant WNW to NW trend (Fig. 6b), with low plunging angles (<30°) both to the NW and SE, despite a large dispersion produced during the D3 folding event. Mesostructures developed during D2 are NW to WNW-trending asymmetrical, isoclinal and often rootless similar-style folds, and ductile shear zones characterized by a planar-linear S2-L2 fabric preserving the early-formed subhorizontal geometry. Towards the tectonic contact between the Namibe Group and the Epupa Complex, S2 exhibits blastomylonitic characteristics (Figs. 7e, 8c, d). In this structural level, D2 fold limbs are invariably intensely boudinaged; boudin orientation and asymmetry (Hanmer and Passchier, 1991) generally indicating a SE-directed, subhorizontal extension parallel to the fold axis. Oblique grain-shape fabrics in quartz aggregates, asymmetrical porphyroclasts and S–C fabrics consistently indicate a top-to-the-SE sense of shearing (Fig. 7f).

D2 deformation developed under greenschist to high-T amphibolite facies metamorphic conditions, attaining the partial melting

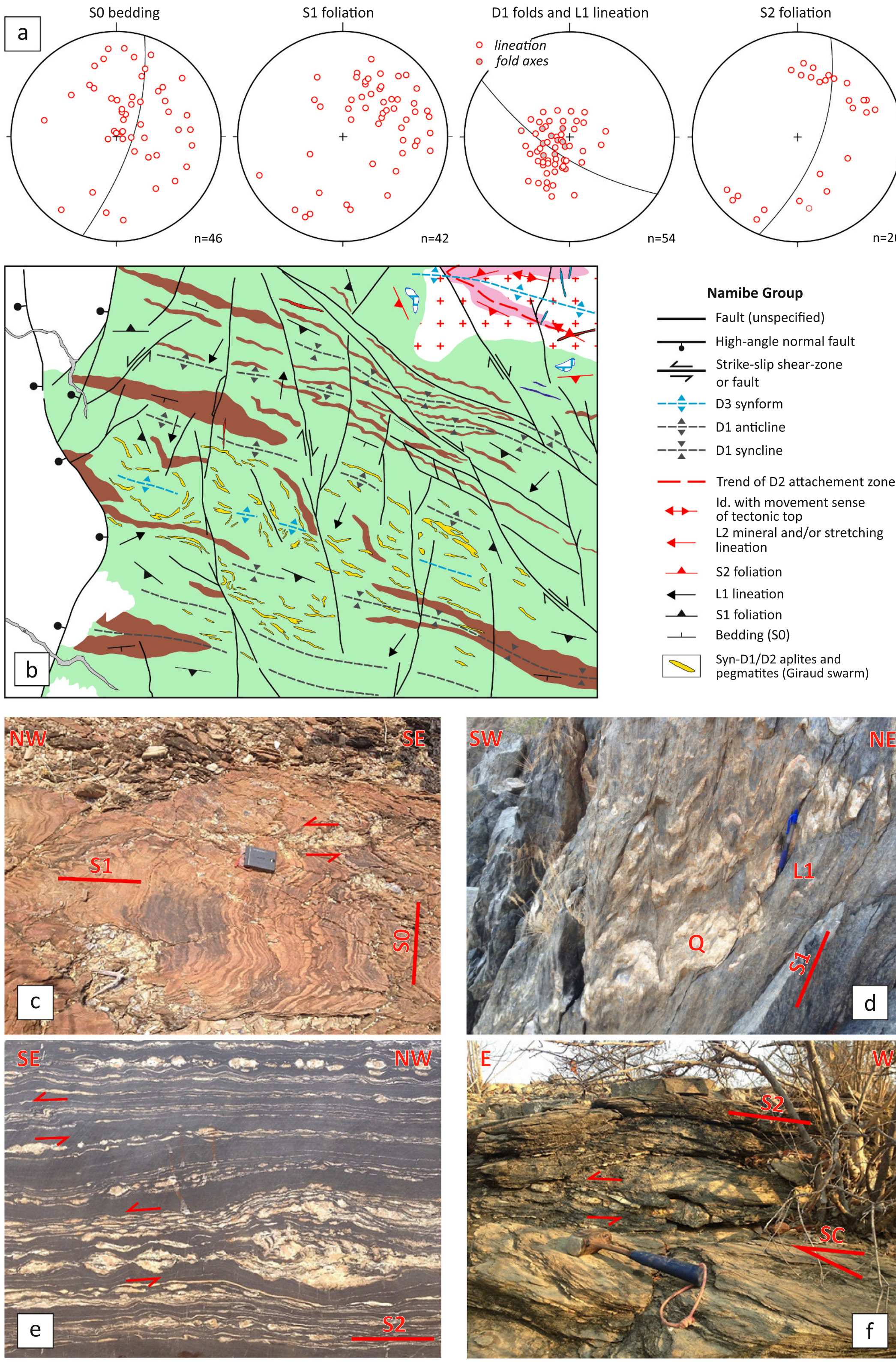

Fig. 7. D1 and D2 structures developed in the Namibe Group in the eastern sector of the Giraul River Valley. (a) Stereographic projection of poles of D1 and D2 structural fabrics. (b) Detailed structural map of D1 folds developed in the Namibe Group. (c) Hinge zone of D1 fold with a steeply plunging fold-axis developed in slates and phyllites of the Namibe Group. Note the subvertical disposition of the S0 bedding and the S1 axial-plane foliation in the D1 fold, as well as metamorphic quartz-veins rotated to S1. Muatampembe sector, near Bero Giraúl summit. (d) Syn-D1 metamorphic quartz-veins (Q), rotated and stretched parallel to S1 during sinistral subvertical shearing. Note the subvertical arrangement of L1. Namibe Group of the Muatampembe sector, near Bero Giraúl summit. (e) Syn-D2 aplitic veins, rotated and stretched parallel to S2 during SE-directed D2 subhorizontal shearing. Namibe Group in the Tamacuala sector, Namibe-Virey road. Field width = 3 m. (f) Mesoscopic S-C structures of D2 undulating a subhorizontal S2 developed in schists of the Namibe Group. Camungua stream. Caraculo-Virey road. (e) and (f) are views in the XY plane of finite strain (i.e., perpendicular to the shear plane and parallel to stretching lineation).

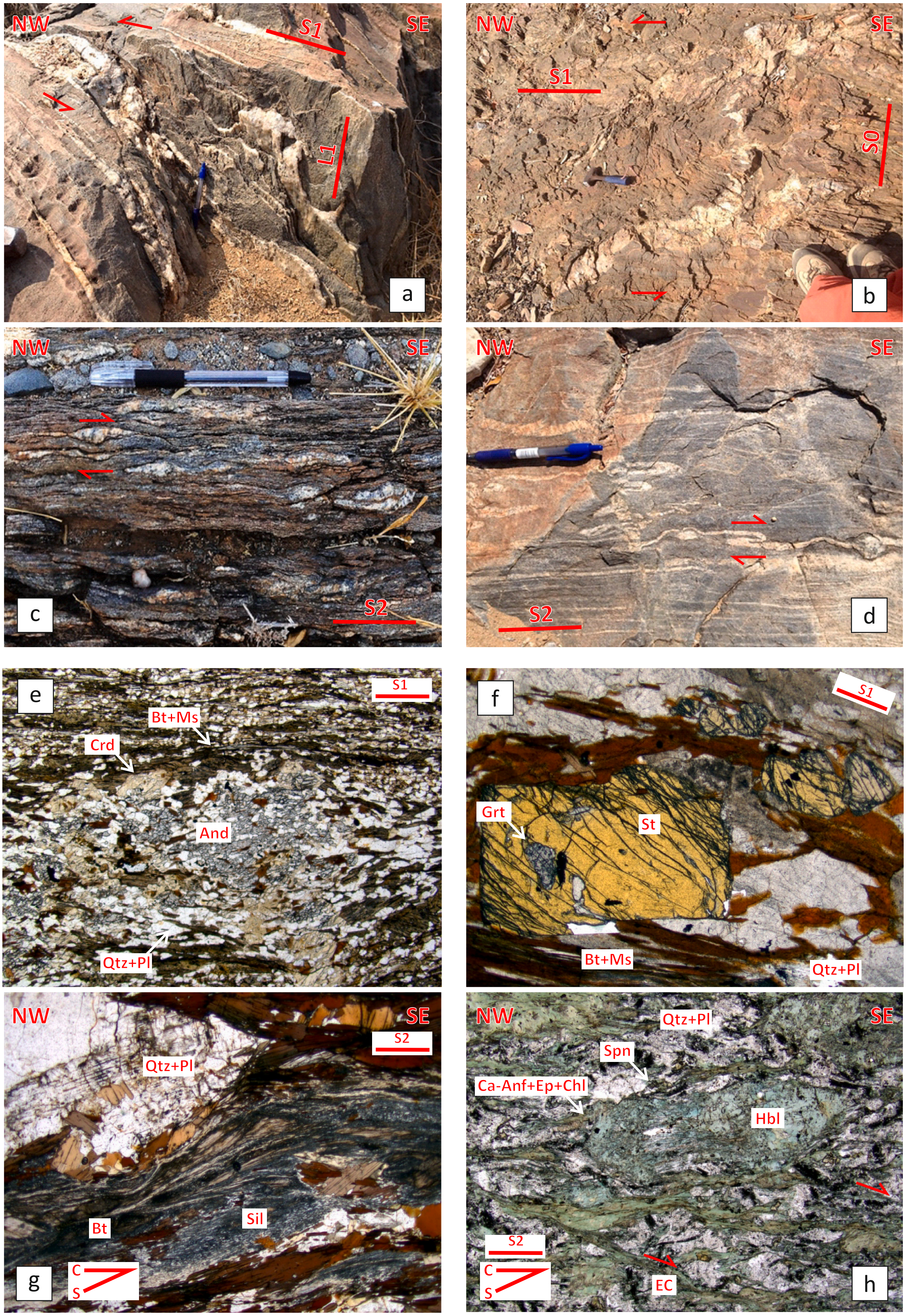

(caption on next page)

Fig. 8. D1 and D2 structures developed in the Namibe Group in the Hiquia River sector. (a) Syn-D1 metamorphic quartz-veins (Q) rotated and stretched to parallelism to S1 during sinistral subvertical shearing. Note the subvertical disposition of L1. (b) Plan view of a quartz-vein rotated during sinistral subvertical shearing of D1 deformation. (c) Quartz-plagioclase veins sheared subhorizontally during D2. The asymmetry of the porphyroclasts and pressure shadows indicates a SE-directed shear sense. (d) Isoclinally folded and boudinaged aplitic veins during D2 subhorizontal shear. The asymmetry of folding and tails around porphyroclasts establishes a top-to-the SE shear sense. Microphotographs: (e) Andalusite (And) poikiloblasts and cordierite (Crd) porphyroblasts (variably pinnitized) surrounded by an S2 foliation marked by biotite (Bt) and muscovite (Ms) lepidoblasts and quartz (Qtz) and plagioclase (Pl) aggregates. PPL. (f) Staurolite (St) porphyroblasts grown on an S2 foliation defined by biotite and muscovite microdomains alternating with quartz and plagioclase-rich microdomains. Note the relict inclusions of garnet (Grt) in the staurolite. PPL. (g) S-C structure developed in sillimanite-bearing micaschists from the lower structural levels of the Namibe Group. Note the elongation with S2 (and L2) of the fibrolitic sillimanite (Sil) aggregates. The asymmetry of the S-C structure establishes a top-to-the SE shear sense. PPL. (h) S-C structure developed in amphibolite from the lower structural levels of the Namibe Group. The S and C planes are defined by calcic amphibole (Ca-Amp), epidote (Ep) and chlorite (Chl), as well as sphene (Sph) aggregates. Note the elongation of a hornblende prism in the S2 planes and the development of pull-aparts perpendicular to the L2 filled with quartz and calcic amphibole. S-C planes are displaced by extensional crenulation (EC) foliation. The asymmetry of the S-C structure and EC planes establishes a top-to-the SE shear sense. PPL. Width of field in microphotographs = 5 mm. PPL = plane polarized light. Mineral abbreviations after Bucher and Frey (2002).

(migmatization) in extensive areas. The field metamorphic gradient increases towards the structurally lower levels located in the core of the D3 anticlines. In basal schists and paragneisses of the Namibe Group, S2 foliation is defined by biotite and muscovite lepidoblasts and L2 lineation by elongated quartz-feldspathic aggregates, fibrolitic sillimanite nematoblasts and pressure shadows around andalusite, cordierite and garnet porphyroblasts (Fig. 8g). The first occurrence of sillimanite in the metapelites allows regional mapping of a syn-D2 isograd of sillimanite + muscovite, which is located close to the contact between the Epupa Complex and the Namibe Group (Escuder-Viruete et al., 2021a). In amphibolite, S2 is defined by the elongation of hornblende, plagioclase and ilmenite aggregates, as well as variable modal contents of clinopyroxene, epidote/clinozoisite, quartz, K-feldspar and calcite (Fig. 8h).

In the stromatic paragneisses of the Epupa Complex, S2 is characterized by leucosome bands of granitic composition parallel to the S2 foliation in the mesosome, suggesting migmatization to have been at least a syn-S2 process (Fig. 9c). This migmatitic S2 foliation is also defined by subparallel centimetric-scale lenses of pegmatite and aplite. During syn-D2 partial melting event, granites and leucogranites of the G1 plutonic suite intruded the Epupa Complex gneisses (Escuder-Viruete et al., 2021a, 2024a, b). These granitoids formed concordant sills to S2, often exhibiting an internal magmatic biotite foliation. The upper structural levels of the Namibe Group were contemporaneously intruded by dykes and sills of aplites and pegmatites of the Giraúl swarm (Fig. 7b).

4.2.4. D3 deformation

D3 deformation is spatially very heterogeneous and D3 fabric elements mainly occurs in the lower structural levels of the Namibe Group and in the Epupa Complex. In the higher structural levels of the Namibe Group, D3 typically produced a shortening orthogonal to S1 and reflattened this structure. D3 is characterized by the formation of open to closed folds with subvertical or moderately NE-vergent axial planes (Fig. 9d). These folds locally developed a widely spaced S3 crenulation foliation (Fig. 9e) and a L3 intersection lineation. The S3 axial planar foliation strikes WNWand is characterized by a consistent high-dip angle to the NE and SW (Fig. 6b). The L3 lineation in these planes exhibits a medium to low-plunge angle towards the NW and SE (Fig. 6b), aligning with the fold-axes of the D3 antiforms and synforms. In stereographic projection, L3 lineations align along a N297°E plane dipping 82° to the NE (Fig. 6b), orthogonal to the NNE trending D4 structures. These features suggest that L3 dispersion is related to the shortening of the subsequent D4 deformation. Deformation event D3 developed under prehnite-pumpellyte and greenschist facies metamorphism in the Namibe Group, and amphibolite facies metamorphism in the Epupa Complex. Depending on the metamorphic grade, S3 is defined in metapelites by a granolepidoblastic aggregate of quartz, muscovite and opaques, with variable amounts of prehnite, chlorite, biotite, cordierite and K-feldspar. The presence of leucosomes in the hinge zones of D3 folds and parallel to S3 foliation in the gneisses of the core of D3 antiforms indicates local migmatization persisted during D3. In the Tchicolangita sector, the D3 macrostructure features upright, open antiforms and synforms, with WNW-trending fold-axes, essentially parallel with L2 (Fig. 9b). In summary, the D3 macrostructure regionally folds the S2 foliation, the D2 shear zone subparallel to the contact between the Namibe Group and the Epupa Complex, and the leucogranite sills of the G1 plutonic suite.

4.2.5. D4 deformation

D4 is a very heterogeneously developed and poorly penetrative deformation. It is restricted to NNE-SSW trending bands, particularly near granitic intrusions of G3 plutonic suite (Fig. 5; Escuder-Viruete et al., 2021a, 2024a, b). Cartographically, D4 event produced inflections in the trace of competent quartzite and metacarbonate layers and the S1 foliation in the supracrustal rocks of the Namibe Group. D4 mesostructures further comprise folds with a NNE-SSW to a less frequent NNW-SSE trend and a subvertical axial plane, accompanied by the development of a spaced S4 foliation (Figs. 6b, 9f). In metapelites, S4 is defined by the elongation of sericite, chlorite and opaque minerals, with variable modal contents of calcite. In slates and schists, D4 produced two conjugate arrays of subvertical kink-bands trending NW-SE and NE-SW, indicating a W to WNW-directed subhorizontal shortening. There is no evidence for partial melting during D4 deformation.

5. Geochronology

The objective of undertaking U-Pb SHRIMP and $^{40}Ar/^{39}Ar$ geochronology was to date the protoliths of selected samples, the thermal peak of the Eburnean metamorphism and the subsequent cooling events. The orthogneisses and paragneisses samples from the Epupa Complex were prepared in the IGME-CSIC Laboratories (Tres Cantos, Madrid). Analytical work and age dating was carried out in the IBERSIMS Laboratories (U-Pb SHRIMP, University of Granada) and the Pacific Center for Isotopic and Geochemical Research (University of British Columbia, Canada). Additional information such as sample location, analytical procedures applied with each geochronological technique used and isotopic data obtained are reported by Escuder-Viruete et al. (2021a) and in the Supplementary Material S1, S2, S3, S4 and S5. Samples are identified by two codes: namely the field code and the PLANAGEO database code (in parentheses).

5.1. U-Pb SHRIMP geochronology

Unravelling the history of migmatitic ortho and paragneisses of the Epupa Complex involves determining the ages of the protolith, subsequent deformation and metamorphic overprint. Prior to analysis, cathodoluminescence (CL) images of individual zircons were used to select the part of zircon cores and rims intended for analysis. The rims could represent newly grown metamorphic or magmatic anatectic zircon. To avoid mixed domains, the smaller 10 mm spot beam was used to sample smaller domains, compensating the larger analytical uncertainty with a better spatial resolution. Where possible, the standard 20 mm diameter

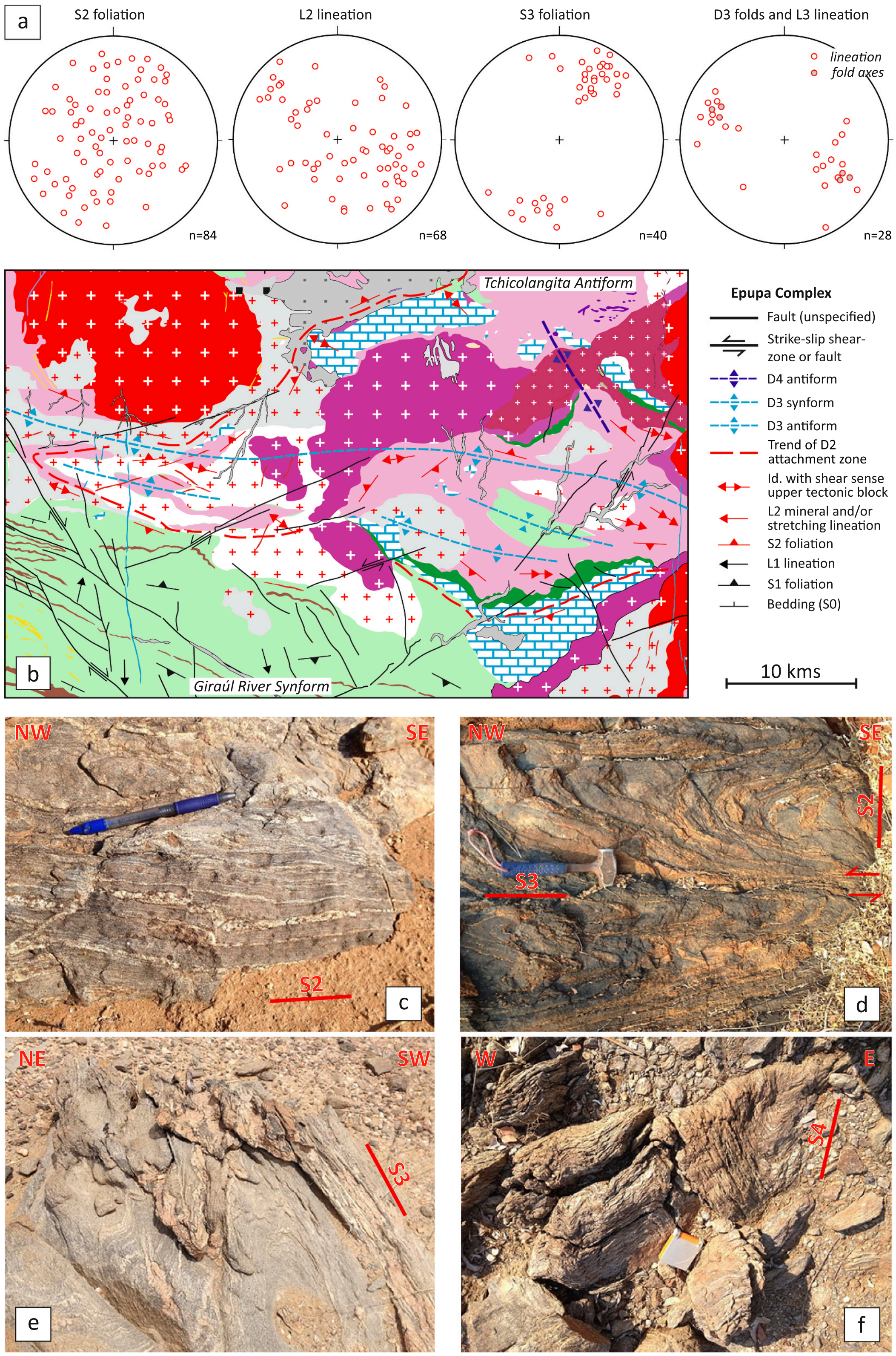

Fig. 9. D3 macrostructure developed in the Tchicolangita sector. (a) Stereographic projection of poles of D2 and D3 structural fabrics. (b) Detailed structural map of D3 Tchicolangira antiform, composed by upright, open antiforms and synforms developed in the Epupa Complex. (c) Granitic leucosome veins with syn-D2 garnets developed in garnet-bearing paragneisses. Note the parallelism of the veins with the S2 foliation in the paragneiss. Epupa Complex, Capolopopo antiform. (d) D3 folds deforming S2 foliation developed in an amphibolite of the Namibe Group. Note the sinistral shearing on the fold limbs with formation of a S3 foliation. Catuite stream, Caraculo-Virey road. (e) Tight, asymmetric and NE-verging D3 folds deforming a S2 foliation in migmatitic paragneisses of the Epupa Complex. Note the folding of syn-S2 leucosomes and the development of a spaced S3 in the axial plane. Curoca-Iona road. Field width = 1.5 m. (f) Angular folds formed during D4 in the shales and phyllites of the Namibe Group in the Chitangala sector, north of Virey.

spot was used. In-situ U-Pb zircon geochronology in high-grade metamorphic belts is complicated by Pb loss, newly grown or overprinted zircon and analytical uncertainties. Those could result in wide arrays of data points overlapping the U-Pb Concordia curve on concordant/sub-concordant positions (Corfu, 2013). This requires a careful approach similar to that described by Spencer et al. (2016) for unmixing detrital zircon ages. For Paleoproterozoic zircon the highest precision and chronometric power lies in the $^{207}Pb/^{206}Pb$ age. In this case, the discordancy of the data is assessed to stablish potential discordancy lines. If such lines have a lower intercept above the origin of the Concordia curve, such as a Paleozoic lower intercept, then the significance of the $^{207}Pb/^{206}Pb$ ages of the discordant data is compromised. This is because it will skew the data towards a younger age. In this study a cut-off of less than 2.5 % discordancy was used to treat $^{207}Pb/^{206}Pb$ ages as concordant. The $^{207}Pb/^{206}Pb$ age density plots of the “concordant” data are used to deconvolute overlapping age clusters using Density Plotteŕs

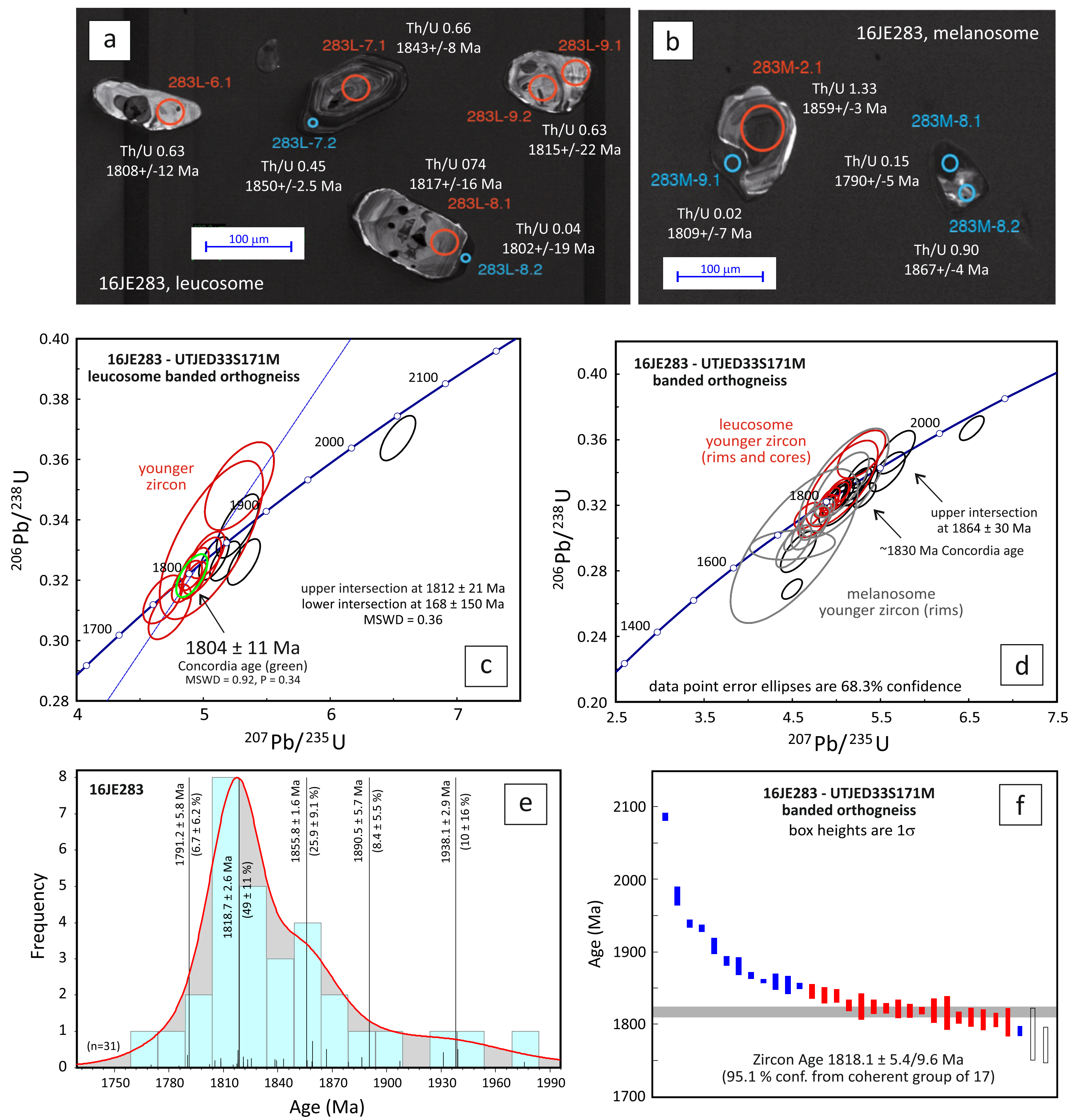

Fig. 10. U-Pb SHRIMP Concordia diagrams for zircons extracted from samples of the the Epupa Complex, in which error ellipses are 1σ. Cathodoluminescence photographs of zircon crystals analyzed in the (a) leucosome and (b) melanosome of the 16JE283 banded orthogneiss. Red circle, 20-µm diameter spot analysis; blue circle, 10-µm diameter spot analysis. Circles are scaled to their diameter. Zircon ages in the (c) leucosome and (d) melanosome of the same banded orthogneiss. Note the greater age range in the melanosome, which includes inherited zircons. (e) $^{207}Pb/^{206}Pb$ KDE age distribution of the most concordant zircons (<2.5 % discordant) analyzed in the banded orthogneiss. (f) Age provided by the *TuffZirc* algorithm using the leucosome and the melanosome zircon data. See text for discussion.

mixture model (Vermeesch, 2012). For the Kermel Density Estimation (KDE) and the probability density plot (PDP) a bin width of 25 Ma is used; this value is set by the analysis with the largest uncertainty. Concordia ages and/or upper intercept ages, anchored by concordant clusters, in conjunction with the zircon CL images and the individual Th/U ratios provide backup to separate older protolith from younger metamorphic/magmatic anatectic ages. This is consistent with a low Th/U ratio (<0.1) proxy for migmatitic zircon (Yakymchuck et al., 2018).

5.1.1. Banded biotitic orthogneiss

Sample 16JE283 (UTJED33S171M) is a banded biotitic orthogneiss from the northern limb of the D3 Tchicolangite antiform in the Epupa Complex (Fig. 5). The sample exhibits a penetrative S2-L2 planar-linear fabric, which is slightly folded by metric-scale D3 folds and displaced by subvertical shear zones parallel to the regional axial-plane S3. The orthogneiss contains leucogranitic leucosomes with granular texture, oriented parallel to the S2 and locally to the S3 axial plane of D3 folds. Samples from melanosome and leucosome bands were processed separately in order to isolate newly grown anatectic zircons from older zircons in the protolith (Fig. 10a, b). Older zircons are potentially well-preserved in the melanosome. Zircon analyses (n = 36) from both melanosome and leucosome bands provide a continuous cluster of "concordant" ages overlapping the Concordia curve between 1800 and 1950 Ma (Fig. 10d). Three core analyses providing 2025 Ma and 2450 Ma ages (not shown) are indicative of older zircon xenocrysts. The $^{207}Pb/^{206}Pb$ KDE age distribution of the most concordant zircons (<2.5 % discordant) shows a skewed distribution with a major peak at 1818 Ma, a smaller "hump" at 1855 Ma and tailing towards 1900 Ma, which coincide with the major and lesser peaks of the bimodal PDP distribution (Fig. 10e).

The age of the protolith is difficult to assess from the available data. The concordant zircons from the melanosome (<2.5 % discordant) provide a Concordia age of ~1830 Ma, while the entire zircon data yield an upper intersection age of 1864 ± 30 Ma (Fig. 10d). This suggests that the presence of a mixture of younger anatectic ca. 1.81 Ga zircons and older 1.86–1.95 Ga zircons in the data set. Cathodoluminescence images of zircons reveal the preservation of individual crystals with zoned rims and cores of ~1.85 Ga age in both the leucosome and the melanosome portions of the banded orthogneiss. Therefore the "hump" at 1855 Ma in the KDE distribution of the $^{207}Pb/^{206}Pb$ ages (Fig. 10e) might be the best approximation to the age of the protolith.

The migmatization event is assessed using the youngest zircons from the leucosome. These zircons preserve cathodoluminescence bright concentric cores and discrete dark outer rims. The analyses of the rims and cores overlap each other defining a Concordia age of 1804 ± 11 Ma (MSWD 0.92) and an upper intersection age of 1812 ± 21 Ma (Fig. 10c). This supports the magmatic anatectic growth of new zircon in the leucosome at ca. 1810 Ma. Zircons from the melanosome are different from old zircons cores, which preserve partial reabsorption with a new dark zircon overgrowth in the outer rim, providing a relatively young age of 1810 Ma. The dark outer rims on zircons from both leucosome and melanosome have low Th/U ratios, generally < 0.1 (Fig. 10b). Combining the leucosome and the melanosome rim zircon data, Isoploťs *TuffZirc* algorithm provides an age of 1818.1 + 5.4 Ma/−9.5 Ma (Fig. 10f). This is interpreted as the age of the growth of anatectic zircon, the S2 migmatitic foliation during the thermal peak of the Eburnean metamorphism, and the intrusion of syn-D2 anatectic leucogranites (G1 plutonic suite).

5.1.2. Stromatic pelitic paragneiss

Sample 16JE92 (UTJED33S037M) is a stromatic pelitic paragneiss from the southern limb of the Tchicolangite antiform of the Epupa Complex, situated near the contact with the basal marbles and amphibolites of the Namibe Group (Fig. 5). This paragneiss is rich in biotite and sillimanite, whose alignment define a S2-L2 planar-linear fabric parallel to granitic leucosomes formed during syn-D2 migmatization. This fabric preserves a superimposed solid-state deformation involving shearing subparallel to S2, which was developed under high-T amphibolite facies conditions. Zircons from this paragneiss provided one Mesoarchean (3.1 Ga), four Neoarchean (2.6–2.4 Ga) and eighteen Paleoproterozoic (2.07–1.85 Ga) concordant and discordant ages (Fig. 11a, b). Cathodoluminescence images show a variety of older Archean and Paleoproterozoic zircon types (Fig. 11a), with no clear evidence of reabsorption and new growth of younger zircon. There is a very thin outer ribbon of bright zircon and, in grains such as 16JE92-4.1 (Fig. 11a), there is a growth of a dark outer rim with a low Th/U ratio. This U-rich rim returned the most discordant analysis due to Pb-loss, potentially representing metamorphic zircon overgrouth. Given their small width, it was not possible to conduct SHRIMP analysis. Archean zircons are likely to have been inherited from the sedimentary protolith, whereas Paleoproterozoic zircons formed during the Eburnean orogeny. In the Fig. 11c, the Paleoproterozoic zircons define three age groups: 2.07–2.02 Ga, 1.97–1.95 Ga, and 1.87–1.85 Ga. The first and third groups allow us to obtain concordant ages of 2071 ± 9 and 1856 ± 12 Ma. The Concordia 1856 ± 12 Ma age represents the most recent or maximum depositional age for sedimentation of the protolith of the paragneiss.

5.1.3. Pelitic paragneiss

Sample 16JE187 (UTJED33S113M) is a stromatic pelitic paragneiss collected in the core of the D3 Capolopopo antiform in the Epupa Complex (Fig. 5). The paragneiss is characterized by a non-coaxial S2-L2 planar-linear fabric defined by granitic leucosome bands with a granular texture, resulting from "in situ" syn-D2 partial melting. D2 deformation produced isoclinal folds, shear zones subparallel to S2, and high-T amphibolite facies mineral assemblages composed of quartz + plagioclase + K-feldspar + biotite + sillimanite + garnet. The majority of 28 zircons analyzed present in cathodoluminescence images bright concentric cores and dark outer rims overgrowths with low Th/U ratios. Three discrete analyses returned inherited cores with 1.94 to 1.96 Ga ages. The remaining core and rim zircon analyses define a Discordia line with an upper intercept age of 1811 ± 20 Ma (MSWD 0.20; Fig. 11d). Dark outer rims are U-rich and more discordant due to late Pb-loss. As such, 1811 ± 20 Ma is interpreted to mark the age of zircon growth during the D2 event and the thermal peak of the metamorphism, including partial melting responsible for granitic leucosomes.

In summary, the new zircon growth during the thermal peak of metamorphism and associated partial melting of the Epupa complex occurred at 1.80–1.82 Ga, which is typical to occur during high-grade metamorphism (e.g., Yakymchuk et al., 2018). In cathodoluminescence images (Figs. 9, 11), the characteristic bright zircon cores with elevated Th/U ratios and the dark Th/U-poor zircon rims are indicative of initial zircon crystallization from an anatectic melt and a subsequent formation of monazite concomitant to a sharp decrease in the Th/U ratio (<0.1) during crystallization of the outer rim (Fig. 11e). The older cores extracted from melanosomes attest that zircon was partially dissolved during anatexis and new zircon with low Th/U ratios grew coincidentally with the late stage of zircon growth. In the case of the stromatic paragneiss 19JE92, the anatectic process might have been so short-lived that no partial dissolution of zircon was achieved and only a very thin outer rim might developed around some zircons. This scenario allowed the preservation of a wide variety of zircon with different textures and ages.

5.2. $^{40}Ar/^{39}Ar$ geochronology

Muscovite from the stromatic pelitic paragneiss 16JE92 (UTJED33S037M) provided a plateau age of 1798.1 ± 8.5 Ma (MSWD = 0.40 and probability = 0.75) for six steps in the incremental heating (i.e. from 3 to 8) and the 50.3 % of the ^{39}Ar released (Fig. 12a). This plateau age is equivalent to the integrated age (weighted average) of 1798.3 ± 6.0 Ma, obtained for the same increments of the spectrum. The age

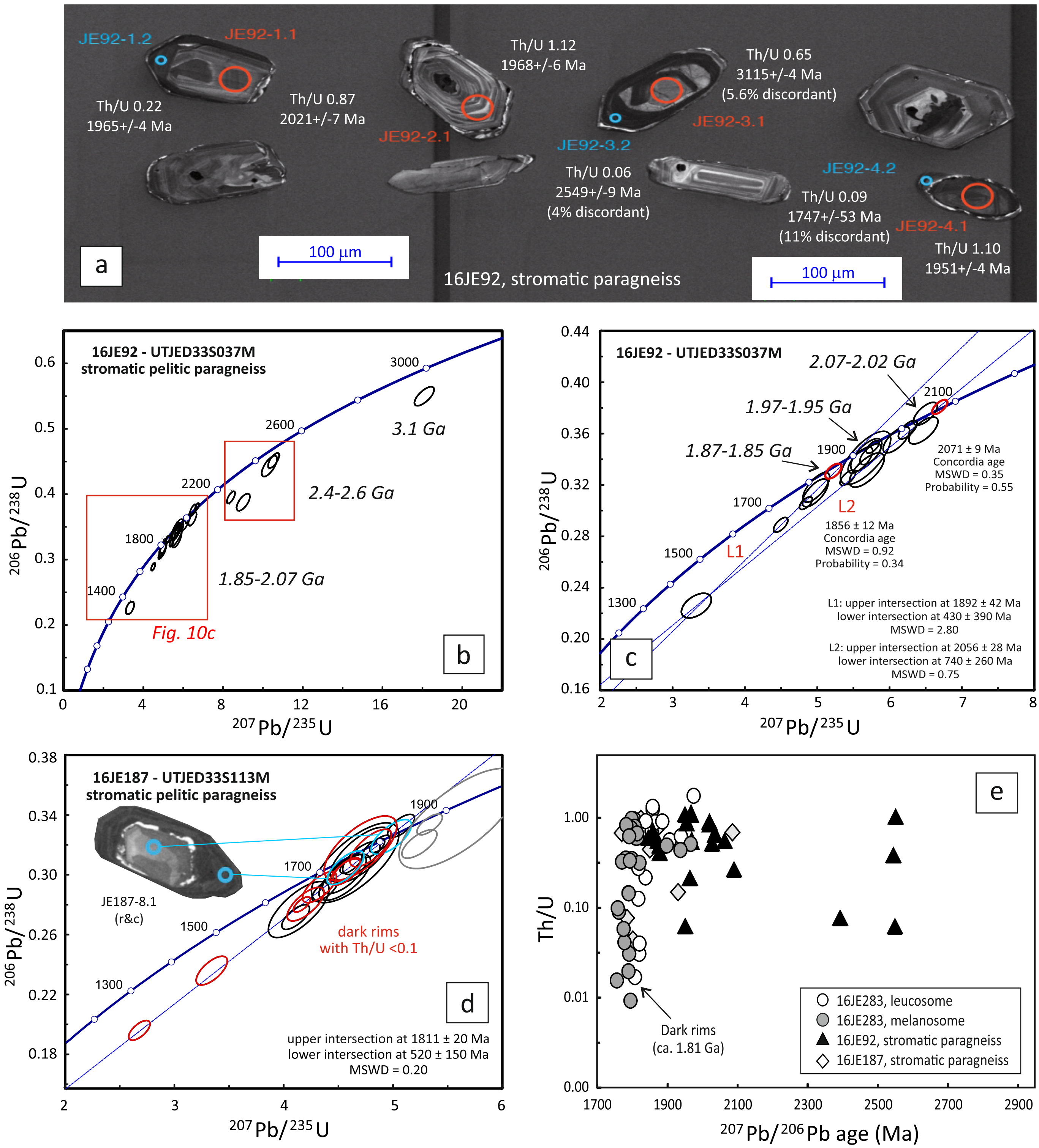

Fig. 11. U-Pb SHRIMP Concordia diagrams for zircons extracted from samples of the Epupa Complex, in which error ellipses are 1σ. (a) Cathodoluminescence photographs of zircon crystals analyzed in the 16JE92 sample of stromatic pelitic paragneiss. (b) Mesoarchean (3.1 Ga), Neoarchean (2.6–2.4 Ga) and Paleoproterozoic (2.07–1.85 Ga) zircons ages obtained in the 16JE92 sample of stromatic pelitic paragneiss. Zircons of Archean ages are interpreted to be inherited from the sedimentary protolith and zircons of Paleoproterozoic ages were formed during the Eburnean orogeny. Red circle, 20-µm diameter spot analysis; Blue circle, 10-µm diameter spot analysis. Circles are scaled to their diameter. (c) Detail of the Paleoproterozoic zircon ages in the 16JE92 sample that define three groups: 2.07–2.02 Ga, 1.97–1.95 Ga, and 1.87–1.85 Ga. (d) Late Eburnean zircon ages obtained in the 16JE187 sample of stromatic pelitic paragneiss. (e) Diagram of Th/U versus $^{207}Pb/^{206}Pb$ age in the analyzed zircons. See text for discussion.

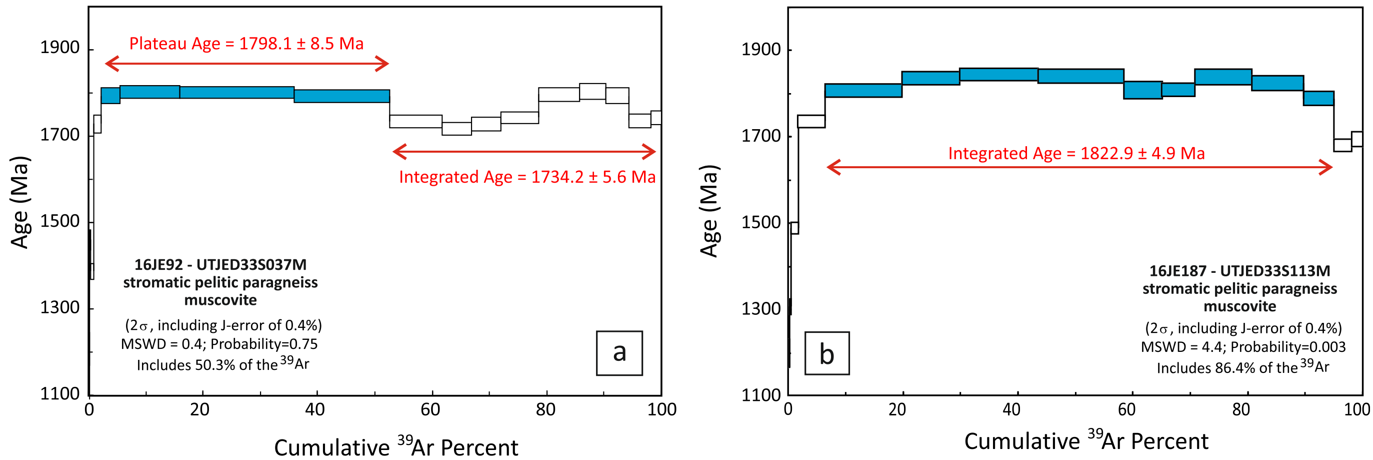

Fig. 12. $^{40}Ar/^{39}Ar$ spectra for mineral separates obtained in samples from the Epupa Complex. The uncertainty of the ages is 2σ and includes those of the monitor and decay constant. See text for discussion.

spectrum also shows a thermal history disturbed by a 1734.2 ± 5.6 Ma event, as indicated by the integrated age (weighted average) of the nine youngest increments (i.e. from 9 to 17). The inverse isochron method for these steps provided an age of 1773.3 ± 9.5 Ma (MSWD = 0.36 and probability 0.87), with a high uncertainty due to the error in the initial ^{40}Ar-^{36}Ar ratio (see Escuder-Viruete et al., 2021a). The plateau age is interpreted as a cooling age to a temperature lower than 350–400 °C (muscovite closure temperature; Hodges, 2003), shortly after the syn-D2 high-grade metamorphic peak, indicating a rapid exhumation of the Epupa Complex.

In the 16JE187 (UTJED33S113M) sample of stromatic pelitic paragneiss, muscovite occurs as large lepidoblasts elongated parallel to S2 foliation. Muscovite separated from this sample provided an integrated age of 1822.9 ± 4.9 Ma (MSWD = 4.4, probability = 0.003) for nine increments (i.e. from 5 to 13) of the 86.4 % of the ^{39}Ar released (Fig. 12b). Ages obtained in six of these steps by the normal and inverse isochron methods are 1794 ± 39 Ma (MSWD = 5.0) and 1783 ± 25 Ma (MSWD = 4.4), respectively, despite a large error due to the initial ^{40}Ar-^{36}Ar value (see Escuder-Viruete et al., 2021a). The integrated age is within the error of the U-Pb SHRIMP age obtained from zircons (1810 ± 19 Ma), dating the thermal peak of syn-D2 Eburnean metamorphism, under sillimanite + K-feldspar stability conditions. Therefore, the integrated age of ~1823 Ma represents a cooling age at T < 350–400 °C, shortly after the thermal peak of metamorphism and partial melting of the paragneiss. The latter is interpreted to represent rapid exhumation of the Epupa Complex.

6. Discussion

6.1. Basement-cover relationships

The presence of paragneiss enclaves in the orthogneisses and augengneisses in the Epupa Complex confirms the interpretation that paragneisses constitute the host where the granitic protoliths intruded in the Paleoproterozoic. Inherited zircons establish emplacement ages between 2.05 and 1.95 Ga for the protoliths of the orthogneisses. Kröner et al. (2010, 2015) and Kröner and Rojas-Agramonte (2017) provide Nd isotopic data from the Epupa Complex in Namibia suggesting the 2.4–2.0 Ga evolution of the protoliths of the orthogneisses from the mantle. For these authors, these protoliths are igneous rocks of calc-alkaline composition, formed in an Eburnean continental volcanic arc of about 2.0 Ga age, built on the southern margin of the Congo Craton. These calc-alkaline granitoids would have been deformed, metamorphized and migmatized during advanced episodes of the Eburnean orogeny.

In the Namibe region, cartographic relationships, different lithological constituents, occurrence of basal polymictic conglomerates in the northeastern sector of the sedimentary basin (Serra da Chicallungo), monocyclic orogenic character, and absence of orthogneiss intercalations indicate that the Namibe Group was unconformably deposited over the Epupa Complex. The existence of a mafic magmatism towards the base of the Namibe Group, recorded by the amphibolite and metavulcanite protoliths (Gutierrez-Medina, 2021), suggests that the sedimentary basin was formed during crustal extension and related partial melting of the mantle. In the central and southwestern sectors of the basin, initial deposition of carbonate protoliths of the calcitic and dolomitic marbles, was followed by the accumulation of thick and monotonous sequence of siliciclastic rocks. Preserved sedimentological characteristics indicate deposition in the feeding channels and depositional lobes of a submarine turbidite system (e.g., Bouma, 2004). The composition of the channeled facies conglomerate clasts points to source regions of granitic and quartzite composition, as well as to a rapid transport to the depositional site facilitated by turbidity currents. Taking into account the inherited zircons ages obtained in the Epupa Complex paragneisses of the ages of the regional Eburnean metamorphism, the depositional age of the Namibe Group is constrained between 1.97–1.95 and 1.85–1.83 Ga.

6.2. Structural and metamorphic evolution

Structural data at all scales indicate that the Epupa Complex and the Namibe Group underwent D1 to D4 polyphase ductile deformation and regional metamorphism, which led to partial melting conditions in large sectors during the Eburnean orogeny. In the Namibe region, this polyphase deformation transposed structures formed during early tectonometamorphic events in the Epupa Complex, as no clear related relics have been found.

In the supracrustal metasedimentary rocks of the Namibe Group, D1 event produced a km-scale structure consisting of WNW to NW-trending folds with variably NNE-directed vergence, which fold S0 bedding planes and giving rise to a subvertical axial-plane S1 foliation and a steeply plunging L1 intersection lineation. Sheared and folded mesoscopic quartz-veins indicate that D1 deformation involved a sinistral transpressive regime that produced a NE to NNE-trending shortening orthogonal to S1, a subvertical stretching parallel to L1 and syn-D1 metamorphic mineral assemblages, resulting in a crustal thickening (Fig. 13). This transpression was partitioned at the mesoscale in bulk pure shear-dominated deformation in low-strain lenses surrounded by simple shear-dominated deformation in sinistral subvertical shear zones. In the Epupa Complex, only relics mesostructures produced by D1 have

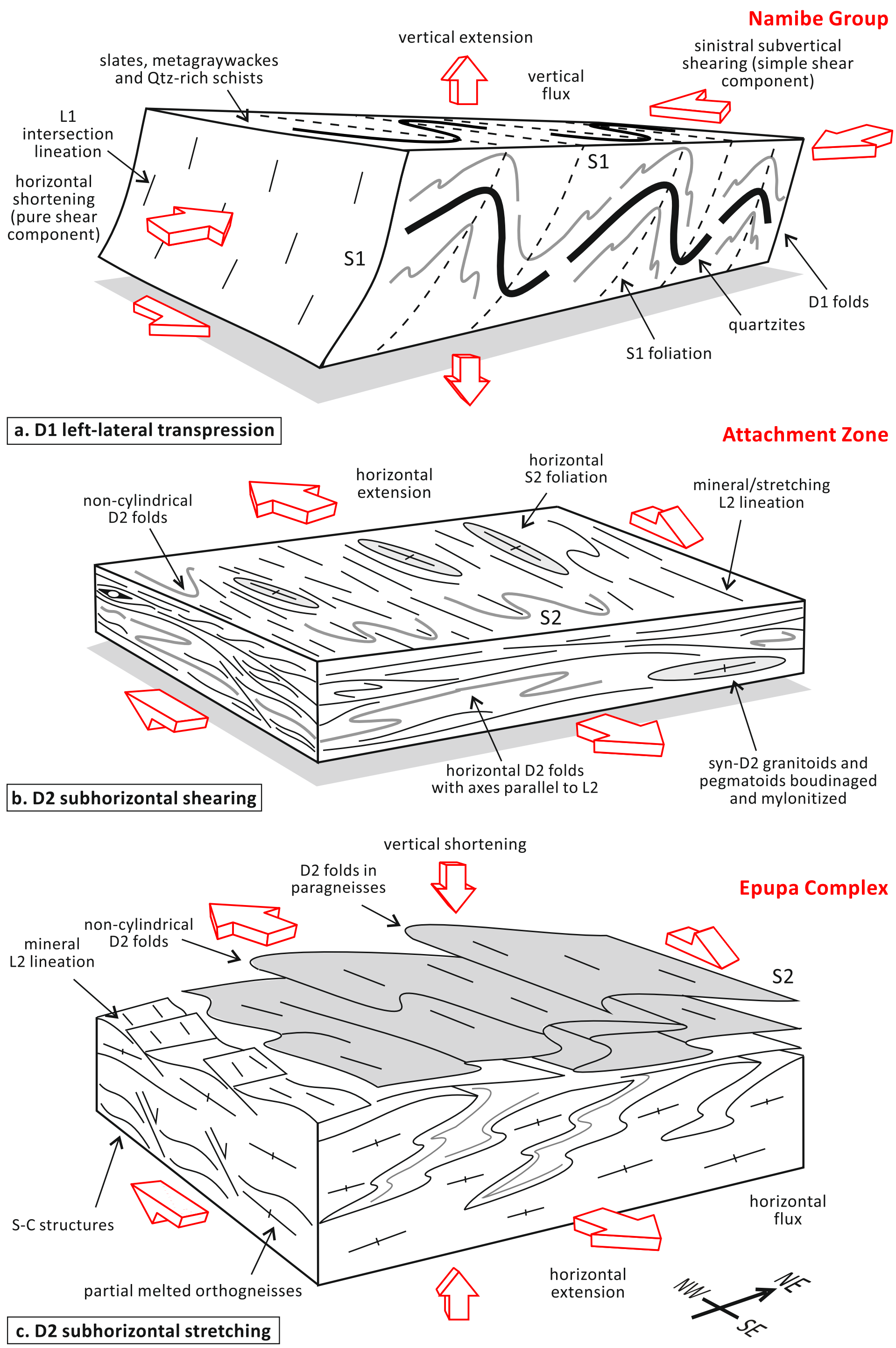

Fig. 13. (a) Diagram showing the interpretation of the D1 deformation based on the structures developed in the Namibe Group. The D1 sinistral transpression produced NNE-directed horizontal shortening and vertical stretching. The resulting D1 macrostructure consists of a large-scale, NE-verging vertical folding of the Namibe Group metasediments. Diagram showing the interpretation of the D2 deformation based on the structures developed in the attachment zone (b) and in the underlying Epupa Complex (c). D2 consisted of a horizontal shearing that produced vertical shortening and horizontal extension. Except in the lower structural levels of the Namibe Group, no development of penetrative D2 structures has been observed in the superstructure. The formation of the attachment zone and the vertical partitioning of deformation was probably controlled by the strong rheological contrast between the underlying partial melting orthogneisses and the overlying lower grade metasediments. For clarity, the effects of late deformations D3 and D4 have been omitted in the diagrams.

been recognized.

Deformation event D2 produced S2-L2 planar-linear fabrics and ductile shear zones subparallel to the contact between the metasedimentary rocks of the Namibe Group and the gneisses of the Epupa Complex, which constituted a subhorizontal high-strain zone. Therefore, D2 deformation reworked the unconformity between the Epupa Complex and the Namibe Group. Towards the lower structural levels of the Namibe Group, S1 appears folded and microcrenulated within S2 microlithons. At these structural levels and in the underlying Epupa Complex, D2 deformation produced the transposition of the previous fabrics to S2 and was accompanied by the formation of leucosome bands parallel to S2. D2 deformation was also accompanied by the emplacement of sills and veins of aplites, pegmatites and leucogranites concordant with S2 foliation.

Prograde metamorphism coeval with D1 and D2 attained greenschist to amphibolite facies conditions (Ms ± Chl ± Bt ± Grt ± St ± And/Sill ± Crd) in the Namibe Group and upper amphibolite facies conditions (Sill + Kfs ± Crd ± Grt mineral assemblages) in the Epupa Complex. The D2 deformation led to lateral displacement and extrusion of the of the Epupa Complex at a regional scale by NW-SE subhorizontal stretching with SE-directed shearing (Fig. 13). This mesocrustal lateral flow was kinematically compatible with the NE-trending orthogonal shortening of the upper crustal metamorphic rocks of the Namibe Group. Therefore, the D2 transition zone between the Epupa Complex and the Namibe Group can be considered as a ductile attachment zone in the sense of Teyssier et al. (2002), Tikoff et al. (2002, 2004) and Teyssier and Cruz (2004), allowing kinematical compatibility between different deformation modes in the orogenic crust. The subhorizontal D2 attachment zone developed in the middle crust kinematically resolves the oblique shortening of the orogen with subvertical stretching in the upper Namibe Group and subhorizontal flow in the lower Epupa Complex. The upper structural limit of the attachment zone locates the sillimanite isograd and the beginning of the partial melting processes, resulting in a high thermal gradient. Therefore, the highest strain of D2 deformation was located along the attachment zone, where a strong rheological contrast existed between the more competent metasedimentary rocks of the upper Namibe Group and the less competent partially molten gneisses of the lower Epupa Complex (Fig. 13). This rheological contrast favored the formation of domes in the Epupa Complex during D2 and D3, and allowed the exhumation by buoyancy of the partially molten middle crust.

Deformation D3 was more heterogeneous in affecting the Namibe Group and the Epupa Complex. It produced WNW to NW-trending folds with NNE/NE vergence, and was responsible for the regional-scale antiformal and synformal macrostructures. In the Namibe Group, S1/S2 is locally crenulated by a spaced S3 foliation developed at greenschist to amphibolite facies conditions. In the Epupa Complex, D3 gave rise to a subvertical S3 and a crenulation L3 plunging a low-angle to the NE and SE, parallel to the trace of the antiforms. The presence of leucosome bands parallel to S3 and towards the contact with the syn-D3 granitoids indicate local upper amphibolite facies metamorphism and associated migmatization during D3 event.

Deformation D4 produced ductile–brittle and poorly penetrative compressional structures along discrete deformational bands. Macroscopically, it produced NNE-trending subvertical folds with a kink geometry, indicating a W to WNW-directed regional shortening.

6.3. Ductile flow in the Eburnean orogenic crust

Coeval transpression of the upper crust and lateral flow of the middle crust has been described in ultra-hot orogens and interpreted as the type of deformation that takes place in a particularly weak lithosphere submitted to oblique convergence (Carnard et al., 2006; Chardon et al., 2009, 2011). Within this structural framework, the transition zone between the superstructure subjected to vertical stretching (thickening) and the coeval lateral flow of the infrastructure, as defined by Vissers (1992) in the Pyrenees, represents an attachment zone that maintains the kinematic compatibility between crustal levels (Tikoff et al., 2002; Teyssier and Cruz, 2004; Chardon et al., 2011; Cochelin et al., 2017).

In the Namibe region, the geometric and kinematic characteristics of D2 deformation indicate that the role of the originally subhorizontal attachment zone was to maintain the vertical strain continuity through the hot Eburnean crust. This strain continuity was accomplished by partitioning the orogen-normal shortening into sinistral vertical shearing and lateral horizontal flow between the superstructure and the infrastructure, respectively. The development of the attachment zone was facilitated by the lithological contrast between the Epupa Complex and the Namibe Group, giving rise to a strong D2 strain and kinematic gradient. In turn, the attachment zone was thermally located in an isotherm, the metamorphic sillimanite isograd, which must have been a rheological threshold in the thickened Eburnean crust. The attachment zone further facilitated the uplift of the partial melted buoyant Epupa Complex into domes during D3 deformation, as well as the emplacement of the syn-kinematic granitoids of the G1 and G2 plutonic suites. In this sense, the development of the attachment zone during D2 and the emplacement of the gneiss domes during D3, absorbed the kinematic discrepancies produced by contrasting deformation modes in the underlying Epupa Complex and the overlying Namibe Group.

The regional syn- to late-D3 transpressive subvertical shear zones crosscut the attachment zone in the limbs of the D3 domes. These shear zones deformed the S2 foliation and reactivated the S3 foliation along retrograde bands. Greenschist facies syn-kinematic mineral assemblages formed in these shear zones attest to cooling during strain localization and hardening. These relationships indicate an increase of the coupling across the attachment zone during the crustal cooling and exhumation of the Epupa Complex during the late-D3 and D4 deformative events (i.e., after 1798.1 ± 8.5 Ma; the latest cooling age in the Epupa Complex).

6.4. Implications of the geochronological data

Fig. 14a shows the frequency diagrams of concordant U-Pb zircon ages obtained in this study from the Epupa Complex ortho and paragneisses. Zircon ages obtained from these samples are largely Paleoproterozoic and to a lesser extent Archean. Seven age groups are defined by the frequency peaks at 3.10, 2.55, 2.40, 2.05, 1.95, 1.85 and 1.82–1.80 Ga, with the latter being the most dominant age group. These age groups are comparable to concordant U-Pb age groups defined from detrital zircons in a fluvial sediment from the Cunene River in Ruacaná (Angola-Namibia border) by Gärtner et al. (2014). The catchment area of the Cunene River covers a relatively large sector of the Southwestern Congo Shield. Although the age frequencies are different, these authors obtain frequency peaks of radiometric ages of 2570, 1964, 1861, 1778 and 1736 Ma, with 1964 Ma being the dominant one (Fig. 14b), as well as others Mesoproterozoic ages (not shown). These authors correlate these populations of U-Pb zircon ages with the main tectonomagmatic and tectonometamorphic events in the history of the Southwestern Congo Shield. These events would be related to the growth of continental crust by orogenic processes, or would result from Archean crustal fragments that were reworked during Paleoproterozoic orogenic events.

Following the supercontinental cycle model of Rino et al. (2004), the most frequent populations of zircons formed during the dispersal of a supercontinent and the amalgamation of its successor (Bradley, 2011; Roberts et al., 2015). From this point of view, different zircon populations in Fig. 14a could be related to the main geodynamic events that involved the Namibe region throughout its geological history. In this sense, the concentration of the 2.55 Ga zircon ages could be related to the breakup of the hypothetical Vaalbara continent between 2.7–2.5 Ga. Subsequently, the continental dispersal during the Paleoproterozoic culminated with the formation of the continent Columbia (or Nuna) between 2.1 and 1.9 Ga. As most zircons returned ages between 2.0 and 1.8 Ga, the emplacement of the igneous and formation of metamorphic rocks of the Namibe region are related to this supercontinental cycle.

The U-Pb SHRIMP geochronological data indicate the existence of a first group of ages between 2600 and 1970 Ma, obtained in inherited xenocrystals or in cores of zoned detrital zircons extracted from the ortho and paragneisses of the Epupa Complex. These results account for the ages of both the source areas of the sedimentary protoliths and the crystallization of the igneous protoliths of the complex. The results obtained in monozircons and overgrown zircon rims in ortho and paragneisses of the Epupa Complex define a second group of zircon ages between 1830 and 1810 Ma. These U-Pb SHRIMP ages are related to the Eburnean tectonometamorphic evolution of the Namibe region. Together with the $^{40}Ar/^{39}Ar$ geochronological results, the ages indicate that the thermal peak of syn-D2 metamorphism and the crystallization of

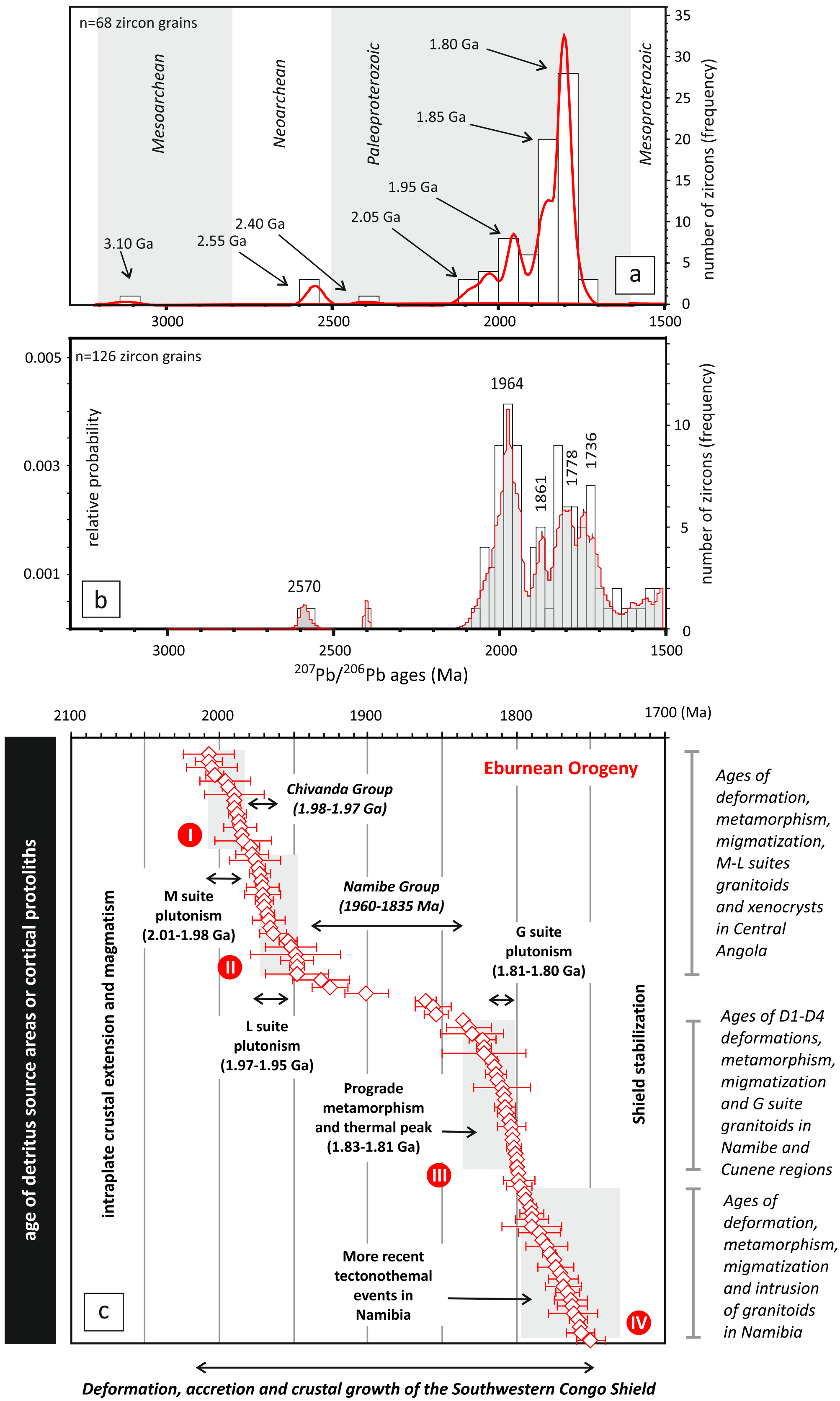

(caption on next page)

Fig. 14. (a) Frequency and probability density diagrams of all the analyzed zircons (n = 68)in the ortho and paragneisses samples of the Epupa Complex. (b) Frequency and probability density diagrams of zircons (n = 126) from an actual fluvial sediment of the Cunene River sampled at Ruacaná (Angola-Namibia border) obtained by Gärtner et al. (2014). All U-Pb ages are concordant with levels between 90 and 110 %, including the average ages calculated for the main age groups. (c) Synthesis of U-Pb ages in zircons obtained by TIMS and SHRIMP in the Paleoproterozoic igneous and metamorphic rocks of the UTE-PLANAGEO Block (southwestern Angola), as well as data of the Southwestern Congo Shield from the regional literature (compiled in Escuder-Viruete et al., 2021a, b, c, 2024; Merino Martínez et al., 2024). The radiometric ages compilation allows to distinguish four Ebunean tectonomagmatic events (I, II, III and IV), accompanied by three high-T and migmatization tectonometamorphic events, but with different geographical development.

leucosomes parallel to S2 foliation (1818.1 + 5.4/−9.5 Ma and 1810 ± 19 Ma), the crystallization of anatectic leucogranites (1808 ± 7 Ma; G1 plutonic suite) and the rapid exhumation of the Epupa Complex at T < 350–400 °C (1822 ± 5 Ma), took place in a short time interval (~10 Ma).

In summary (Fig. 14c), the U-Pb zircon ages obtained by TIMS and SHRIMP techniques from the Paleoproterozoic igneous and metamorphic rocks of the Namibe region (Escuder-Viruete et al., 2021b, c, 2024a, b; Merino Martínez et al., 2024; and references herein) and regional data from the Southwestern Congo Shield (de Wit and Linol, 2015; Jelsma et al., 2018), allows us to propose a tectonomagmatic and tectonometamorphic evolution of the Namibe region during the Eburnean orogeny. This compilation of ages includes at least four Ebunean tectonomagmatic events, namely I, II, III and IV, and three high-T tectonometamorphic events including migmatization, but of variable geographical development.

Event I of ages between 2.01 and 1.98 Ga is recorded by the intrusion of the M plutonic suite in the Kuito and Andulo sector (Escuder-Viruete et al., 2021b), close to the Central Angola Mobile Belt. It also includes inherited xenocrystic zircons in the paragneisses of the Epupa Complex and in relatively younger granitoids, altogether suggesting evolution via crustal reworking processes. The related tectonometamorphic event is characterized by polyphasic penetrative ductile deformation, responsible for cortical thickening and regional medium- and low-P metamorphism (Escuder-Viruete et al., 2021b).

Event II of ages between 1.97 and 1.95 Ga is marked by the intrusion of the L plutonic suite in the Kuito and Andulo sector (Galán-Pérez, 2021). These intrusions indirectly constrain the 1.98–1.97 Ga age for the supracrustal accumulation of the protoliths of the metasedimentary rocks of the Chivanda Group (Galán-Pérez, 2021).

Event III of ages between 1.83 and 1.81 Ma is defined from zircons extracted from the ortho and paragneisses of the Epupa Complex and metasedimentary rocks of the Namibe Group in the Namibe region, as well as the Cunene sector of northernmost Namibia (Escuder-Viruete et al., 2021a). Therefore, the Eburnean magmatism and metamorphism moved geographically from the NE to the SW (present coordinates) during the Eburnean orogeny in the Paleoproterozoic times. This event is related to a tectonometamorphic evolution characterized by polyphase ductile deformation, crustal thickening, regional low-P metamorphism, partial melting and emplacement of anatectic leucogranites of the G1 magmatic suite. These relationships facilitate the proposition of a time window for the sedimentation of the Namibe Group protoliths between 1.97–1.95 and 1.85–1.83 Ga. These metasedimentary rocks were intruded by the G1, G2 and G3 plutonic suites between 1.81 and 1.80 Ga (Fig. 14c; Escuder-Viruete et al., 2021a, 2024). Therefore, the deformation and regional metamorphism developed in the Namibe region were relatively late in the overall Eburnean orogenic evolution. The $^{40}Ar/^{39}Ar$ muscovite ages obtained from the paragneisses overlap within error with the SHRIMP zircon ages for the thermal peak of syn-D2 metamorphism (Event III) and associated formation of S2 leucosomes. This indicates that cooling of the Epupa Complex to temperatures less than 350–400 °C was very rapid. The latter is interpreted to imply a quick exhumation.

Event IV of ages between 1.80 and 1.72 Ma is recorded in the Epupa Complex of the Cunene region and in the basement rocks of the Kaoko Belt. This event is not recorded in the Namibe region. However, it appears to be defined by a population of U-Pb ages in detrital zircons extracted from Mesoproterozoic siliciclastic rocks of SW Angola (the Kamanjab-Namibe-Epupa group of Ferreira et al., 2024). According to Kröner et al. (2010, 2015, 2017), Brandt et al. (2020) and Lehmann et al. (2020), these ages are related to a Eburnean tectonometamorphic event, responsible for ductile deformation, regional metamorphism, migmatization and granitoid intrusion in the northern region of Namibia.

6.5. *Model of tectonic evolution*

Lithostratigraphic, structural and geochronological observations are integrated in a model of tectonic evolution for the Namibe region of the Southwestern Congo Shield during the Event III of the Eburnean orogeny. The evolution begins with a plate divergence that produced rifting in the Shield, crustal extension and the formation of opposite passive margins (Fig. 15a). On the southern faulted margin of the Congo Shield, the thick siliciclastic sequence with turbiditic characteristics of the Namibe Group was deposited within the 1.97–1.95 and 1.85–1.83 Ga time interval. These siliciclastic rocks are unconformably overlying the Epupa Complex of 2.05–1.95 Ga basement rocks. The source regions of the granite and quartzite clastic material were located further to the NE of the Namibe region in the Shield.

With the transition to the plate convergence, an intermediate oceanic domain was consumed by subduction, thus generating a continental volcanic arc on the southern edge of the Congo Shield (Fig. 15b). Vestiges of this volcanic arc are preserved in the Mudorib Complex (1.81–1.73 Ga; Luft et al., 2011) and in other places of the Paleoproterozoic basement of the Kaoko Belt in northern Namibia (Kröner et al., 2010, 2015).

The docking of the continental margin of the Kalahari Craton to the subduction zone produced continental collision, compressional deformation and crustal thickening (Fig. 15c; see proposed evolution of the Kalahari Craton of Oriolo and Becker, 2018). In the Namibe region, collisional tectonics gave rise to vertical partitioning of the shortening in the crust, which was resolved by the NE-directed D1 sinistral transpression in the suprastructure and subhorizontal D2 ductile flow and tectonic escape to the SE in the infrastructure. Associated crustal thickening produced low-P prograde metamorphism and extensive partial melting processes during the metamorphic thermal peak, accompanied by 1.83–1.81 Ga anatectic leucogranites of the G1 plutonic suite (Escuder-Viruete et al., 2024a, b).

The cessation of convergence gave way to plate divergence that produced extensional tectonics, crustal thinning and exhumation of the deep crustal levels in the orogen (Fig. 15d). In the Namibe region, these processes gave rise to late D3 and D4 deformation events, rapid exhumation of the middle crust, retrograde metamorphism and the intrusion of the 1.81–1.80 Ga G2 and G3 plutonic suites.

7. Conclusions

The main conclusions of this work are:

(1) The Epupa Complex ortho and paragneisses are lithostratigraphically distinctive from the overlying supracrustal metasediments of the Namibe Group. Cartographic relationships in the Namibe region, lithological characteristics and geochronological data indicate that the Namibe Group was unconformably deposited onto the Epupa Complex basement. The sedimentary basin was formed by crustal extensional processes and was mainly filled by turbidite sediments. Epupa Complex and Namibe Group are part of the Southwestern Congo Shield (de Wit

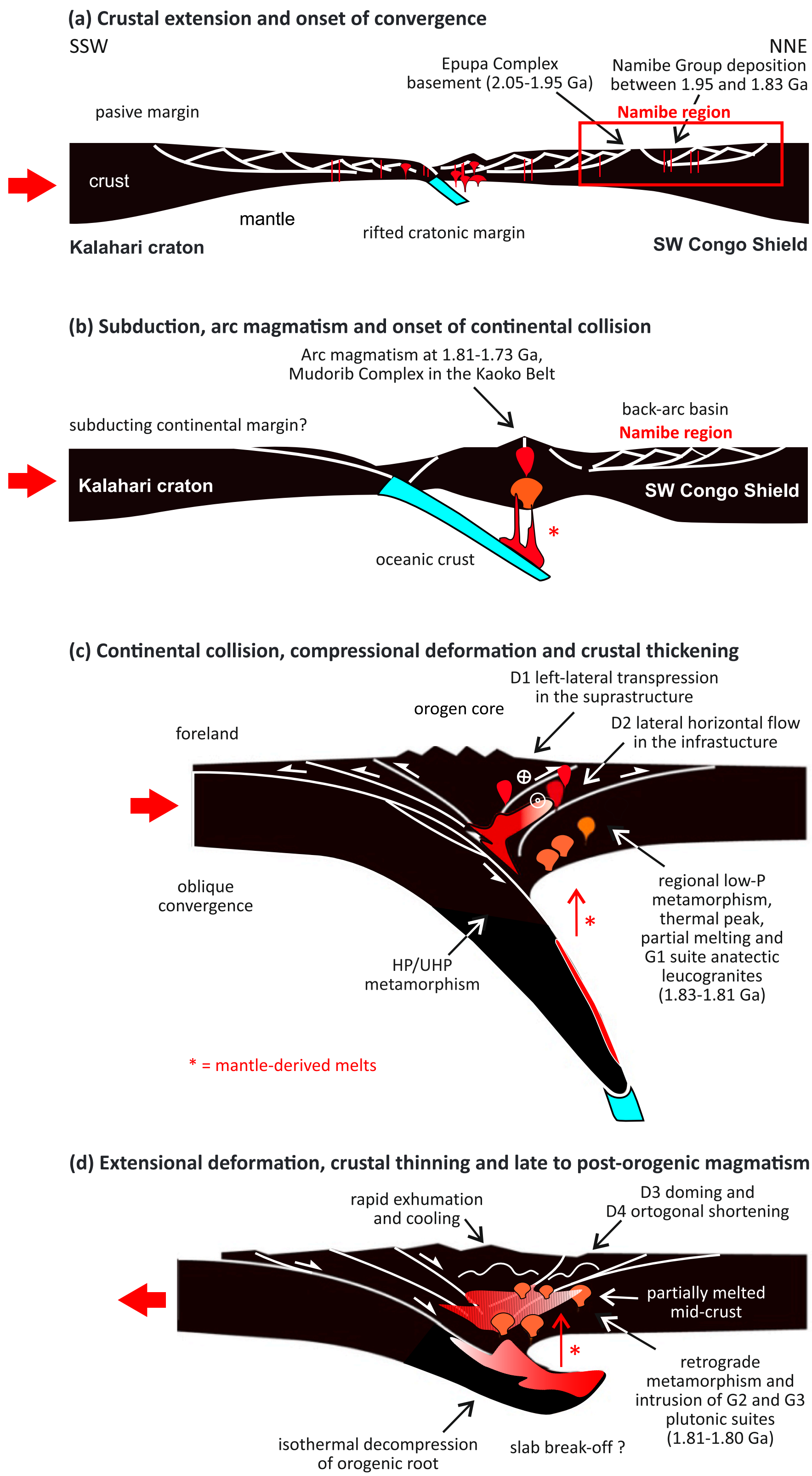

Fig. 15. Simplified tectonic model for the evolution of the Namibe region in the Southwestern Congo Shield during the Event III of the Eburnean orogeny. See text for explanation.

and Linol, 2015), an Archean-Paleoproterozoic domain subjected to tectono-metamorphic processes during the Eburnean orogeny.

(2) Structural data at all scales indicate that the Epupa Complex basement and the Namibe Group sedimentary cover experienced polyphase ductile deformation (D1 to D4) and regional metamorphism attaining partial melting conditions in large areas during the Eburnean orogeny.

(3) An originally subhorizontal D2 attachment zone maintained the

vertical strain continuity through the hot Eburnean crust and coupled sinistral transpressional shearing in the superstructure with a lateral subhorizontal flow in the infrastructure.

(4) U-Pb SHRIMP geochronological data indicate the existence of a first group of zircons of 2.60 to 1.97 Ga ages, which records the crystallization of the igneous protoliths of the Epupa Complex and the source areas ages of the sedimentary protoliths of the Namibe Group. A second group of zircons of 1.83 to 1.81 Ga ages is related to the Eburnean tectonometamorphic evolution of the Namibe region.

(5) The overlapping U-Pb SHRIMP zircon and $^{40}Ar/^{39}Ar$ muscovite ages indicate that the thermal peak of syn-D2 metamorphism, the crystallization of leucosomes parallel to S2, the emplacement of G1 anatectic leucogranites and the rapid exhumation of the Epupa Complex, took place in a ~ 10 Ma time window.

(6) All these data show the development of the late Eburnean orogeny in the Namibe region of the Southwestern Congo Shield.

Declaration of Generative AI and AI-assisted technologies in the writing process

During the preparation of this work the authors used ARIA OPENAI of OPERA browser in order to improve its readability and language. After using this tool, the authors reviewed and edited the content as needed and take full responsibility for the content of the publication.

CRediT authorship contribution statement

Javier Escuder-Viruete: Writing – original draft, Project administration, Methodology, Investigation, Conceptualization. **Luis Quintana:** Methodology, Investigation. **Aratz Beranoaguirre:** Methodology, Investigation. **Pilar Montero:** Methodology, Investigation, Formal analysis, Data curation. **Janet Gabites:** Methodology, Investigation, Formal analysis, Data curation. **Pablo Valverde-Vaquero:** Writing – review & editing, Methodology, Investigation, Formal analysis, Conceptualization. **Américo da Mata Lourenço Victorino:** Resources, Investigation, Data curation.

Declaration of competing interest

The authors declare the following financial interests/personal relationships which may be considered as potential competing interests: Javier Escuder Viruete reports financial support was provided by Geological Institute of Angola. Javier Escuder Viruete reports financial support was provided by Geological and Mining Institute of Spain. This work is part of the geological mapping conducted in the Namibe and Muninho Quadrangles at a scale of 1:250 000, as part of the PLANAGEO Project financed by the Angolan Goverment. If there are other authors, they declare that they have no known competing financial interests or personal relationships that could have appeared to influence the work reported in this paper.

Acknowledgments

This work honors the memory of Eng. Seca Sousa Cassange, Technical Director of the Geological Institute of Angola (IGEO), as a great promoter of the fieldwork of the PLANAGEO Project in the Namibe region. It is also dedicated to the memory of Gustavo Galán-Pérez, who was an excellent colleague and friend during fieldwork. The authors thank IGEO for permission to publish the results of the Geological Subprogram of the PLANAGEO Project. These thanks are extended to the UTE IGME-LNEG-IMPULSO SA for the support and infrastructures provided during fieldwork in southwest Angola. Detailed and constructive reviews made by Joas Kabete, Jeremie Lehmann and two anonymous reviewers, as well as the editorial work by Marly Babinski, significantly improved the manuscript. This is the IBERSIMS Publication N° 116.

Appendix A. Supplementary data

Supplementary data to this article can be found online at https://doi.org/10.1016/j.precamres.2025.107879.

Data availability

Additional geochronological data are provided in the following files. Supplementary Material S1. Analytical techniques. Supplementary Material S2. Geographical location of geochronological samples. Supplementary Material S3. Results of zircon U-Pb SHRIMP geochronology. Supplementary Material S4. Analysis of the Temora zircon standard. Supplementary Material S5. Summary of ^{40}Ar-^{39}Ar incremental heating experiments of mineral separates and plateau age diagrams.

References

Araújo, A.G., Perevalov, O.V., Jukov, R.A., 1988. Carta Geológica de Angola, Escala: 1:1 000 000. Instituto Nacional de Geologia, Angola.

Araújo, A.G., Guimarães, F., (Coords.), 1992. Geologia de Angola. Notícia Explicativa da Carta Geológica à escala 1/1 000 000. Serviço Geológico de Angola, Luanda, 137 pp.

Boniface, N., Schenk, V., 2012. Neoproterozoic eclogites in the Paleoproterozoic Ubendian Belt of Tanzania: evidence for a Pan-african suture between the Bangweulu Block and the Tanzania Craton. Precambr. Res. 208–211, 72–89.

Boniface, N., Schenk, V., Appel, P., 2012. Paleoproterozoic eclogites of MORB-type chemistry and three Proterozoic orogenic cycles in the Ubendian Belt (Tanzania): evidence from monazite and zircon geochronology, and geochemistry. Precambr. Res. 192–195, 16–33.

Bouma, A.H., 2004. Key controls on the characteristics of turbidite systems. In Lomas, S. A., Joseph, P. (Eds.), Confined Turbidite Systems. Geological Society, London, Special Publications, 222, 9–22.

Bradley, D.C., 2011. Secular trends in the geologic record and the supercontinent cycle. Earth Sci. Rev. 108, 16–33.

Brandt, S., Klemd, R., Okrusch, M., 2003. Ultrahigh-temperature metamorphism and multistage evolution of garnet-orthopyroxene granulites from the Proterozoic Epupa Complex, NW Namibia. J. Petrol. 44, 1121–1144.

Brandt, S., Will, T.M., Klemd, R., 2007. Ultrahigh-temperature metamorphism and anticlockwise PT paths of sapphirine-bearing orthopyroxene-sillimanite gneisses from the Proterozoic Epupa complex, NW Namibia. Precambr. Res. 153, 143–178.

Brandt, S., Klemd, R., 2008. Upper-amphibolite facies partial melting of paragneisses from the Epupa complex, NW Namibia, and relations to Mesoproterozoic anorthosite magmatism. J. Metam. Geol. 26, 871–893.

Brandt, S., Klemd, R., Xie, H., Bobek, P., 2021. Unravelling the PT-t history of three high-grade metamorphic events in the Epupa complex, NW Namibia: implications for the paleoproterozoic to mesoproterozoic evolution of the Congo Craton. Am. J. Sci. 321 (1–2), 235–296.

Bucher, K., Frey, M., 2002. Petrogenesis of Metamorphic Rocks, 7th edition. Springer, Berlin, p. 341.

Cahen, L., Snelling, N.J., Delhal, J., Vail, J.R., 1984. The Geochronology and Evolution of Africa: London. Oxford University Press, p. 512.

Cagnard, F., Durrieu, N., Gapais, D., Brun, J.P., Ehlers, C., 2006. Crustal thickening and lateral flow during compression of hot lithospheres, with particular reference to Precambrian times. Terra Nova 18, 72–78.

Carvalho, H., 1983. Carte et Notice explicative préliminaire sur la géologie d'Angola. Garcia De Orta 6 (1/2), 15–30.

Carvalho, H., 1984. Estratigrafia do Precâmbrico de Angola. Garcia de Orta, Série Geológica., Lisboa 7 (1-2), 1-66.

Carvalho, H., Tassinari, C., Alves, P.H., Guimaraes, F., Simoes, M.C., 2000. Geochronological review of the Precambrian in western Angola: links with Brazil. J. Afr. Earth Sc. 31 (2), 383–402.

Chardon, D., Gapais, D., Cagnard, F., 2009. Flow of ultra-hot orogens: a view from the Precambrian, clues for the Phanerozoic. Tectonophysics 477, 105–118.

Chardon, D., Jayananda, M., Peucat, J.J., 2011. Lateral constrictional flow of hot orogenic crust: Insights from the Neoarchean of south India, geological and geophysical implications for orogenic plateaux. Geochem. Geophys. Geosyst. 12, Q02005. https://doi.org/10.1029/2010GC003398.

Cochelin, B., Chardon, D., Denèle, Y., Gumiaux, C., Le Bayon, B., 2017. Vertical strain partitioning in hot Variscan crust: Synconvergence escape of the Pyrenees in the Iberian-Armorican syntax. Bull. Soc. Géol. Fr. 188, 39.

Degler, R., Pedrosa-Soares, A., Dussin, I., Queiroga, G., Schulz, B., 2017. Contrasting provenance and timing of metamorphism from paragneisses of the Araçuaí-Ribeira orogenic system, Brazil: Hints for Western Gondwana assembly. Gondw. Res. 51, 30–50.

de Wit, M.J., Stankiewicz, J., Reeves, C., 2008. Restoring Pan-African-Brasiliano connections: more Gondwana control, less Trans-Atlantic corruption. In Pankurst, R. J., Trouw, R.A.J., Brito Neves, B.B., de Wit, M.J. (Eds.), West Gondwana: Pre-Cenozoic correlations across the South Atlantic region. Geological Society of London, Special Publications 399–412.

de Wit, M.J., Linol, B., 2015. Precambrian Basement of the Congo Basin and its flanking terrains. In: de Wit, M.J. (Ed.), Geology and Resource Potential of the Congo Basin. Springer-Verlag, Berlin Heidelberg, Regional Geology Reviews, p. 417.

Doucoure, M., de Wit, M.J., Bowring, S., 1999. African craton project: a focus on the West African shield, with new data from the Congo Craton, Central African shield. Unpublished CIGCES Annual Report for De Beers Africa Exploration.
Drüpel, K., Littmann, S., Romer, R.L., Okrusch, M., 2007. Petrology and isotopic geochemistry of the Mesoproterozoic anorthosite and related rocks of the cunene intrusive complex, NW Namíbia. Precambr. Res. 156, 1–31.
Escuder-Viruete, J., Correia, J., Quintana, L., 2021a. Notícia Explicativa da Carta Geológica à esc. 1:250 000 SUL D-33/S e SUL D-33/Z do Namibe. Instituto Geológico de Angola. Ministério de Recursos Minerais e Petróleos. Luanda. 180 pp.
Escuder-Viruete, J., Gumiel, J.C., 2021a. Notícia explicativa da Folha Geológica à escala 1:250 000 de Andulo/SUL C33-X metade Sul. Instituto Geológico de Angola. Ministério de Recursos Minerais e Petróleos, Luanda, p. 210.
Escuder-Viruete, J., Gumiel, J.C., 2021b. Notícia explicativa da Folha Geológica à escala 1:250 000 de Cahama/SUL E33-C-I. Instituto Geológico de Angola. Ministério de Recursos Minerais e Petróleos, Luanda, p. 226.
Escuder-Viruete, J., Valverde-Vaquero, P., Beranoaguirre, A., Montero, P., Plastov, J.M., 2024a. Petrology, structural fabric and geochronology of the granitoid suites from the Namibe region (southwestern Angola): record of the Eburnean tectonomagmatic evolution in the Southwestern Congo Shield. Geo-Temas 20, 1326–1329.
Escuder-Viruete, J., Valverde-Vaquero, P., Beranoaguirre, A., Montero, P., Plastov, J.M., 2024b. Petrology, structural fabric and TIMS U-Pb zircon geochronology of the granitoid suites from the Namibe region (southwestern Angola): record of the Eburnean tectonomagmatic evolution in the Southwestern Congo Shield. Boletín Geológico y Minero 136 (1), 1–32. https://doi.org/10.21701/bolgeomin/136.1/008.
Ferreira, E., Lehmann, J., Rodrigues, J.F., Hayes, B., Merino-Martínez, E., Milani, L., Bybee, G.M., Owen-Smith, T.M., García-Lobón, J.L., Tassinari, C.C., Ueckermann, H., 2024. Zircon U-Pb and Lu-Hf isotopes reveal the crustal evolution of the SW Angolan Shield (Congo Craton). Gondw. Res. 131, 317–342.
Galán-Pérez, G., 2021. Notícia Explicativa da Carta Geológica de Kuito à escala 1:250 000. Instituto Geológico de Angola. Ministério de Recursos Minerais e Petróleos, Luanda, p. 178.
García-Lobón, J.L., Rodrigues, J.F., Merino-Martínez, E., Fernández, J., Carvalho, M.J., Batista, J., Escuder-Viruete, J., Lisboa, V., Martín-Banda, R., Francés, A., Ramalho, E., Martín-Méndez, I., Rey-Moral, C., Feria, M.C., Mochales, T., Ferreira, E., Cuervo, I., Victorino, A.M.L., Manuel, J., 2024. El Plan Nacional de Geología de Angola (PLANAGEO). Geo-Temas 20, 1335.
Gärtner, A., Linnemann, U., Hofmann, M., 2014. The provenance of northern Kalahari Basin sediments and growth history of the southern Congo Craton reconstructed by U–Pb ages of zircons from recent river sands. Int. J. Earth Sci. 103, 579–595.
Gutiérrez-Medina, M., 2021. Notícia Explicativa – Folha Geológica de Munhino Sul D-33/M à E. 1:250 000. Instituto Geológico de Angola. Ministério de Recursos Minerais e Petróleos. Luanda. 218 pp.
Hodges, K., 2003. Geochronology and thermochronology in orogenic systems. In: Heinrich, R., Holland, D., Turekian, K. (Eds.), Treatise on Geochemistry, vols. 3–9. Elsevier Inc., pp. 263–292
Holmes, A., 1951. The sequence of pre-Cambrian orogenic belts in south and central Africa. Report of the 18th Session of the International Geological Congress, Great Britain (1948). In Sandford, K.S., Blondel, F. (Eds.), Part 14. Proceedings of the Association des Sérvices Géologiques Africains, London, 254-269.
Jelsma, H.A., Perrit, S.H., Amstrong, R., Ferreira, H.F., 2011. Shrimp U-Pb zircon geochronology of basement rocks of the Angolan Shield, Western Angola. Abstract, 23rd CAG, Johannesburg, 8th–14th January.
Jelsma, H.A., McCourt, S., Perritt, S.H., Armstrong, R.A., 2018. The Geology and Evolution of the Angolan Shield, Congo Craton. In Siegesmund, S. (Ed.), Geology of Southwest Gondwana, Regional Geology Reviews, 217-239.
Kabette, J.M., McNaughton, N.J., Groves, D.I., Mruma, A.H., 2012a. Reconnaissance SHRIMP U–Pb zircon geochronology of the Tanzania Craton: evidence for Neoarchean granitoid–greenstone belts in the Central Tanzania Region and the Southern East African Orogen. Precambr. Res. 216 (219), 232–266.
Kabette, J.M., Gorves, D.I., McNaughton, N.J., Mruma, A.H., 2012b. A new tectonic and temporal framework for the Tanzanian Shield: implications for gold metallogeny and undiscovered endowment. Ore Geol. Rev. 48, 88–124.
Kröner, A., Rojas-Agramonte, Y., Hegner, E., Hoffman, K.H., Wingate, M.T.D., 2010. SHRIMP zircon dating and Nd isotopic systematics of Paleoproterozoic migmatitiv orthogneisses in the Epupa Metamorphic complex of northwest Namibia. Precambr. Res. 183, 50–69.
Kröner, A., Rojas-Agramonte, Y., Wong, J., Wilde, S., 2015. Zircon reconnaissance dating of Proterozoic gneisses along the Kunene River of northwestern Namibia. Tectonophysics 662, 125–139.
Kröner, A., Rojas-Agramonte, Y., 2017. Mesoproterozoic (Grenville-age) granitoids and supracrustal rocks in Kaokoland, northwestern Namibia. Precambr. Res. 298, 572–592.
Lawley, C.J.M., Selby, D., Condon, D.J., Horstwood, M., Millar, I., Crowley, Q., Imber, J., 2013. Lithogeochemistry, geochronology and geodynamic setting of the Lupa Terrane, Tanzania: Implications for the extent of the Archean Tanzanian Craton. Precambr. Res. 231, 174–193.
Lawley, C.J.M., Selby, D., Condon, D., Imber, J., 2014. Palaeoproterozoic orogenic gold style mineralization at the Southwestern Archaean Tanzanian cratonic margin, Lupa Goldfield, SW Tanzania: Implications from U–Pb titanite geochronology. Gondw. Res. 26, 1141–1158.
Lehmann, J., Bybee, G.M., Hayes, B., Owen-Smith, T.M., Belyanin, G., 2020. Emplacement of the giant Kunene AMCG complex into a contractional ductile shear zone and implications for the Mesoproterozoic tectonic evolution of SW Angola. Int. J. Earth Sci. 109, 1463–1485.
Lindeque, A., de Wit, M.J., Ryberg, T., Weber, M., Chevallier, L., 2011. Deep crustal profile across the Southern Karoo Basin and Beattie magnetic anomaly, South Africa: an integrated interpretation with tectonic implications. South African J. Geol. 114, 265–292.
Luft Jr, J.L., Chemale Jr, F., Armstrong, R., 2011. Evidence of 1.7- to 1.8-Ga Collisional Arc in the Kaoko Belt, NW Namibia. Int. J. Earth Sci. 100, 305–321.
Master, S., Rainaud, C., Armstrong, R., Phillips, D., Robb, L., 2005. Provenance ages of the neoproterozoic Katanga Supergroup (Central African Copperbelt), with implications for basin evolution. J. African Earth Sci. 42 (1–5), 41–60.
Maier, W.D., Rasmussen, B., Fletcher, I.R., Li, C., Barnes, S.J., Huhma, H., 2013. The cunene anorthosite complex, Namíbia, and its satellite intrusions: geochemistry, geochronology, and economic potential. Econ. Geol. 108, 953–986.
McCourt, S., Armstrong, R.A., Jelsma, H., Mapeo, R.B.M., 2013. New U–Pb SHRIMP ages from the Lubango region, SW Angola: insights into the Palaeoproterozoic evolution of the Angolan Shield, southern Congo Craton, Africa. J. Geol. Soc. 170 (2), 353–363.
Merino-Martínez, E., Ferreira, E., Valverde-Vaquero, P., Rodrigues, J.F., Escuder-Viruete, J., García-Lobón, J.L., Beranoaguirre, A., Feria, M.C., Rey-Moral, C., Silva, P.B., González-Cuadra, P., Sousa, J.C., Potti, J., Máximo, J., Gutiérrez-Medina, M., Gumiel, J.C., Galán, G., Mochales, T., Manuel, J., Cordeiro, D., Tassinari, C., Montero, P., Sato, K., Fuenlabrada, J.M., Galindo, C. 2024. Edades U-Pb en el sur del Escudo de Angola e implicaciones en la evolución del Complejo de Cunene durante el Mesoproterozoico. Geo-Temas 20, 1350 pp.
Milani, L., Lehmann, J., Bybee, G.M., Owen-Smith, T.M., Oosthuizen, L., Delport, P., Ueckermann, H., 2022. Geochemical and geochronological constraints on the mesoproterozoic red granite suite, Kunene AMCG complex of Angola and Namibia. Precambr. Res. 379, 106821.
Milesi, J.P., Toteu, S.F., Deschamps, Y., Feybesse, J.L., Lerouge, C., Cocherie, A., Penaye, J., Tchameni, R., Moloto-A-Kenguemba, G., Kampunzu, H.A.B., Nicol, N., Duguey, E., Leistel, J.M., Saint-Martin, M., Ralay, F., Heinry, C., Bouchot, V., Doumnang, J.C., Mbaigane, V., Kanda KulaChene, F., Monthel, J., Boutin, P., Cailteux, J., 2006. An overview of the geology and major ore deposits of Central Africa: Explanatory note for the 1:4,000,000 map ''Geology and major ore deposits of Central Africa''. J. Afr. Earth Sc. 44, 571–595.
Miller, R.McG., 2008a. The Geology of Namibia, Vol. I (Archaen to Mesoproterozoic). Ministry of Mines and Energy, Geological Survey Namibia, Windhoek, 631 pág.
Miller, R.McG., 2008b. The Geology of Namibia, Vol. II Neoproterozoic to lower Palaeozoic. Geological Survey of Namibia, Windhoek, 631 pág.
Nagudi, B., Koeberl, C., Kurat, G., 2003. Petrography and geochemistry of the Singo granite, Uganda, and implications for its origin. J. African Earth Sci. 36 (1–2), 73–87.
Nkoumbou, C., Barbey, P., Yonta-Ngouné, C., Paquette, J.L., Villiéras, F., 2013. Pre-collisional geodynamic context of the southern margin of the Pan-African fold belt in Cameroon. J. African Earth Sci. 99, 245–260.
Oriolo, S., Becker, T., 2018. The Kalahari Craton, Southern Africa: From Archean Crustal Evolution to Gondwana Amalgamation. In Siegesmund, S., Basei, M., Oyhantçabal, P., Oriolo, S. (Eds.) Geology of Southwest Gondwana. Regional Geology Reviews. Springer, Cham. doi:10.1007/978-3-319-68920-3_6.
Pereira, E., Tassinari, C.G., Rodrigues, J.F., Van-Dúnen, V., 2011. New data on the deposition age of the volcano-sedimentary Chela Group and its Eburnean basement: implications to post-Eburnean crustal evolution of the SW of Angola. Comunicações Geológicas Do LNEG 98, 29–40.
Pereira, E., Rodrigues, J., Tassinari, C.G., Van-Dúnen, M.V., 2013. Geologia da região de Lubango, SW de Angola - Evolução no contexto do cratão do Congo. Edições LNEG 160. ISBN 978-989-675-031-2.
Rino, S., Komiya, T., Windley, B.F., Katayama, I., Motoki, A., Hirata, T., 2004. Major episodic increases of continental crustal growth determined from zircon ages of river sand; implications for mantle overturns in Early Precambrian. Phys Earth Planet 146, 369–394.
Roberts, N.M.W., Van Kranendonk, M., Parman, S., Shirey, S., Clift, P.D., 2015. Continent formation through Time. Geol. Soc. Lond. Spec. Publ. 389, 197–225.
Seth, B., Kröner, A., Mezger, K., Nemchin, A.A., Pidgeon, R.T., Okruscha, M., 1998. Archean to Neoproterozoic magmatic events in the Kaoko belt of NW Namibia and their geodynamic significance. Precambr. Res. 92, 341–363.
Seth, B., Armstrong, R.A., Brandt, S., Villa, I.M., Kramers, J.D., 2003. Mesoproterozoic U-Pb and Pb-Pb ages of granulites in NM Namibia: Reconstructing a complete orogenic cycle. Precambr. Res. 126, 147–168.
Seth, B., Armstrong, R.A., Büttner, B., Villa, I.M., 2005. Time constraints for Mesoproterozoic upper amphibolite facies metamorphism in NW Namibia: a multi-isotope approach. Earth Planet. Sci. Lett. 230, 355–378.
Spencer, C.J., Kirkland, C.L., Taylor, R.J.M., 2016. Strategies towards statistically robust interpretations of *in-situ* U-Pb zircon geochronology. Geosci. Front. 7 (4), 581–589.
Stankiewicz, J., de Wit, M., 2013. 3.5 billion years of reshaped Moho, southern Africa. Tectonophysics 609, 675–689.
Teyssier, C., Tikoff, B., Waters, C., 2002. Attachment between brittle and ductile crust at wrenching plate boundaries. In Bertotti, G., Schulmann, K., Cloetingh, S. (Eds.), Continental Collision and the Tectono-sedimentary Evolution of Forelands. European Geophysical Society Special Publication, 1, 93-117.
Teyssier, C., Cruz, L., 2004. Strain gradients in transpressional to transtensional attachment zones. In Grocott, J., Mccaffrey, K.J.W., Taylor, G., Tikoff, B. (Eds.), Vertical Coupling and Decoupling in the Lithosphere. Geological Society, London, Special Publications 227, 101-115.
Tegtmeyer, A., Kröner, A., 1985. U–Pb zircon ages for granitoid gneisses in northern Namibia and their significance for Proterozoic crustal evolution of southwestern Africa. Precambr. Res. 28, 311–326.
Thiéblemont, D., Liégeois, J.P., Fernandez-Alonso, M., Ouabadi, A., Le Gall, B., Maury, R., Jalludin, M., Vidal, M., Ouattara-Gbélé, C., Tchaméni, R., 2016.

Geological map of Africa at 1:10 M scale. CGMW-BRGM Editions. https://doi.org/10.14682/2016GEOAFR.
Thiéblemont, D., Callec, Y., Fernandez-Alonso, M., Chène, F., 2018. A Geological and Isotopic Framework of Precambrian Terrains in Western Central Africa: An Introduction. S. Siegesmund et al. (eds.), Geology of Southwest Gondwana, Regional Geology Reviews 107-132.
Tikoff, B. Teyssier, C., Waters, C., 2002. Clutch tectonics and the partial attachment of lithospheric layers. In Bertotti, G., Schulmann, K., Cloetingh, S. (Eds.), Continental Collision and the Tectono-sedimentary Evolution of Forelands. European Geophysical Society Special Publication 1, 119-144.
Tikoff, B., Russo, R., Teyssier, Ch., Tommasi, A., 2004. Mantle-driven deformation of orogenic zones and clutch tectonics. In Grocott, J., Mccaffrey, K.J.W., Taylor, G., Tikoff, B. (Eds.), Vertical Coupling and Decoupling in the Lithosphere. Geological Society, London, Special Publications 227, 41-64.
Vermeesch, P., 2012. On the visualisation of detrital age distributions. Chem. Geol. 312–313, 190–194.
Vissers, R.L.M., 1992. Variscan extension in the Pyrenees. Tectonics 11, 1369–1384.
Waele, B.D., Lacorde, M., Vergara, F., Chan, G., 2015. New insights on Proterozoic tectonics and sedimentation along the peri-Gondwanan West African margin based on zircon U–Pb SHRIMP geochronology. Precambr. Res. 259, 156–175.
Yakymchuk, C., Kirkland, C.L., Clark, C., 2018. Th/U ratios in metamorphic zircon. J. Metamorphic Petrol. 36, 715–737.